DRY DEPOSITION OF NITROGEN CONTAINING SPECIES

Gregory J. McRae and Armistead G. Russell

Environmental Quality Laboratory 206-40
California Institute of Technology
Pasadena, California 91125

Paper presented at

American Chemical Society
183rd National Meeting
Las Vegas, Nevada
March 28 - April 2, 1982

Division of Environmental Chemistry
Symposium on Acid Precipitation
Session on Deposition Both Wet and Dry
Chairman: Dr. B. B. Hicks

ABSTRACT

Nitrogen oxides (NO_x) emissions and the oxidation products formed by photochemical interactions in the atmosphere are responsible for a significant fraction of both dry and wet acid deposition fluxes. In this paper a vertically-resolved, Lagrangian trajectory model is used to predict the diurnal variation of: NO, NO_2, NO_3, HONO, $HONO_2$, HO_2NO_2, RONO, $RONO_2$, RO_2NO_2, N_2O_5 and PAN over an urban airshed. Particular attention is given to the fate of nitric acid and its reaction with gaseous ammonia to form, aerosol phase, ammonium nitrate. A simple model for estimating the deposition fluxes of these species is also presented. A study of the fate of nitrogen oxides emissions, in the South Coast Air Basin of southern California, is used to illustrate the procedures.

I. INTRODUCTION

During the last decade considerable attention has been devoted to understanding the sources, causes and environmental impacts of air pollution. Recently, increased research efforts have been devoted to one particular aspect of this problem - surface deposition of acidic materials. In an urban atmosphere the major precursors of acid deposition are sulfur dioxide (SO_2) and nitrogen oxides (NO_x). These gases and their acidic oxidation products form a heterogeneous mixture of compounds that ultimately return to the earth's surface as either wet or dry deposition. While much of the initial work has been directed at measuring ecosystem acidification by wet precipitation[1,2] there is a growing recognition that other mechanisms, especially dry deposition, are important[3,4].

If the adverse effects of dry deposition are to be minimized through the implementation of source controls then there is a clear need for a formal methodology that can describe the emission, transport, and subsequent fate of acidic compounds and their precursors. One technique, and the approach adopted here, is to use a mathematical model that incorporates the major processes influencing acid deposition. A particular focus of this work is a study of the physical and chemical transformations of NO_x emissions. There are several reasons for this emphasis. One is that the dynamics of nitric acid and ammonia has a dominant influence on surface acidity. Another, and perhaps the most important, is that with changing fuel usage patterns and control of SO_x emissions nitrogen oxides will be a major component of the acid deposition problem.

II. A MODEL OF ATMOSPHERIC TRANSPORT AND CHEMISTRY

Four basic elements determine the pattern of acid deposition: source emissions, atmospheric transport, physical and chemical transformations, and ultimately, the mode of surface removal. While there are several possible frameworks for integrating these processes one of the most useful is provided by the integral form of the atmospheric diffusion equation. Based on a mathematical statement of mass conservation this model provides a simple means for describing the formation and transport of chemically reacting species in the turbulent planetary boundary layer[5,6,7]. Consider a typical airshed of volume V, bounded by a surface A as shown in Figure 1. Over this region the mass balance can be written in the form

$$\frac{\partial}{\partial t}\iiint_V c_i dv + \iint_A F_b^i \cdot \hat{\underset{\sim}{n}} dA = \iiint_V R_i dV \qquad (1)$$

where $c_i(\underline{x},t)$; i=1,...,n is the concentration of species i, $F_b^i(\underline{x},t).\hat{\underline{n}}$ is the mass flux normal to the airshed boundary and $R_i(c_1,\ldots,c_n,T)$ is the rate of chemical production of species i at temperature T. One important property of (1) is that it explicitly shows how the flow of material across the airshed boundaries influences the ambient concentration dynamics. This feature is particularly useful in deposition studies. For example, whether the ground acts as a net source or sink for pollutant material can be determined by simply evaluating the surface integral over the lower boundary of the airshed.

While the mass balance framework provides a convenient framework for calculating acid deposition fluxes, by itself, it is not sufficient. A complete problem formulation requires a characterization of each term in (1) as well as the specification of the associated initial

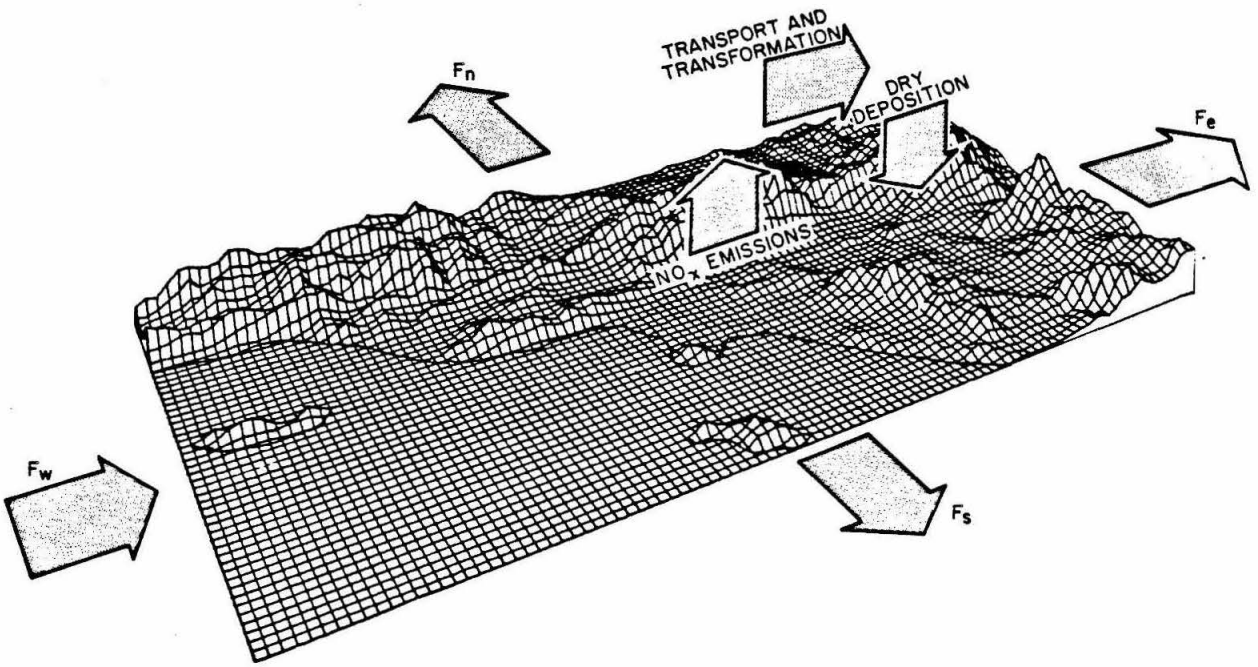

FIGURE 1

Perspective Plot of South Coast Air Basin of Southern California
(The arrows correspond to the processes considered
in the nitrogen mass balance calculations)

and boundary conditions. There are many different ways to establish the initial concentration field.

$$c_i(\underline{x},0) = c_i^o(\underline{x}); \quad i=1,\ldots,n \qquad \underline{x} \in V \tag{2}$$

One simple procedure, and the approach employed in this study, is to use interpolation techniques[8,9].

Several factors, including the nature of the flow field and the surface orientation, influence the way in which the boundary flux $F_b^i(\underline{x},t).\hat{\underline{n}}$ in (1) is characterized. For example, in a turbulent flow field the material flux out of the region, in a direction parallel to the ground, is given by[5]

$$F_b^i.\hat{\underline{n}} = [\underline{u}(\underline{x},t)c_i(\underline{x},t) - \underline{K}\nabla c_i(\underline{x},t)].\hat{\underline{n}} \tag{3}$$

where $\underline{u}(\underline{x},t)$ is the prescribed flow field, and $\underline{K}$ is an eddy diffusivity description of turbulent mixing. (The variations of $\underline{K}$ and $\underline{u}$ as a function of atmospheric stability and surface conditions is described in McRae et al.[5,10] and will not be repeated here.) The magnitude of the fluxes through the top of the airshed depend on the elevation of the boundary. If the height of the airshed is defined to be greater than the maximum extent of the convective mixed layer then the contribution from turbulent transport across the upper boundary is neglible. At ground level, the formulation of the boundary flux $F_b^i(\underline{x},t).\hat{\underline{n}}$, must account for the effects of surface deposition, diffusive transport, and direct emissions of species c_i. A differential statement of mass continuity at the surface is given by

$$v_g^i c_i - K_{zz} \frac{\partial c_i}{\partial z} = E_i(\underline{x},t) \tag{4}$$

where E_i the source emission flux of species i, v_g^i the deposition

velocity and K_{zz} is the vertical transport contribution from turbulent diffusion. Deposition velocities are used to describe the interaction of gases and aerosols with the surface. In general, while more reactive species have a higher deposition velocity, the flux also depends on the meteorological conditions. Subsequent sections of this work are devoted to a more detailed treatment of the surface deposition processes.

One of the most important influences on airshed concentration dynamics is the chemical kinetics, $R_i(c_1,\ldots,c_n,T)$. The development of a mechanism that accurately describes the chemistry occuring in the atmosphere and which at the same time is computationally tractable is a complex undertaking. The task is complicated by the need to maintain a balance between the level of chemical detail and minimizing, for numerical reasons, the number of species and reaction pathways. In this study the photochemistry is based on the mechanism developed by McRae et al.[5], Falls and Seinfeld[11], Falls et al.[12] and Russell et al.[13]. Those reactions that involve nitrogenous species are described in a subsequent section where particular attention is given to the fate of nitric acid and its reaction with ammonia to form, aerosol phase, ammonium nitrate.

Once the various components of the model have been specified then it can be solved in a manner that enables particular species to be traced from their source to their ultimate removal. Unfortunately, in many practical applications, the cost of calculating the flux distribution over a large airshed can be very high[6,14]. There is however, an inexpensive alternative. Under some conditions it is possible to discern the patterns of acid deposition by calculating the flux balances

in columns of air that move across the airshed with the mean flow (Figure 2). For this Lagrangian technique to be valid the effects of horizontal diffusion and vertical wind shear on pollutant distributions must be neglible[15]. Both of these conditions are implicit in the meteorological fields used in this project.

III. SURFACE DEPOSITION OF ATMOSPHERIC CONTAMINANTS

An important component of any approach to estimating the magnitude of acid deposition (and, similarly, acid neutralizing species) is a procedure for calculating the pollutant flux to the surface. This section provides a brief summary of a technique introduced in McRae et al.[5]. In most models the deposition rate is described by a single quantity, the pollutant deposition velocity, v_g. (The species index has been dropped to simplify the subsequent notation.) The flux of material, F, directed towards the lower boundary surface is defined by

$$F = v_g \, c(z_r) \qquad (5)$$

where $c(z_r)$ is the concentration of the material at some reference height z_r. A basic problem with this expression is that it does not explicitly represent the fact that dry deposition involves a complex linkage between turbulent diffusion in the surface boundary layer, molecular scale motion at the air-ground interface and chemical interaction of the material with the surface[16-25]. Various physical processes are involved including gravitational settling, turbulent and molecular diffusion, inertial impaction, phoretic and electrical effects. In addition to these removal phenomena, deposited material can be desorbed or mechanically resuspended.

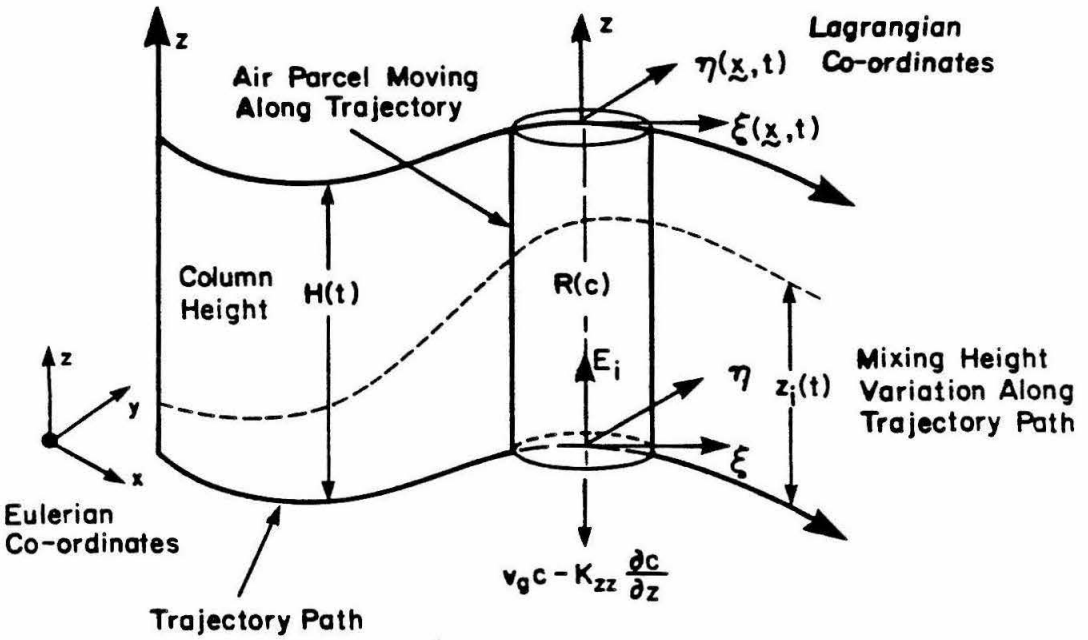

(a)

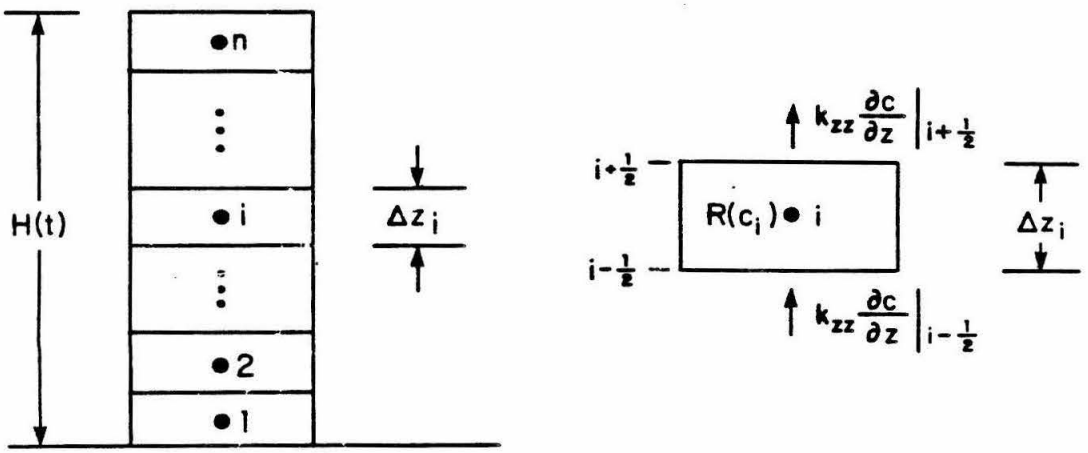

(b)

FIGURE 2

Schematic Representation of
(a) Vertically Resolved Lagrangian Trajectory Model
and (b) the Computational Grid Cell Convention

As a first step towards improving the simple model (5) it is necessary to recognize that there are two basic components associated with pollutant removal: one is the transport of material to the ground and the other is the interaction of the pollutants with the surface. Unless extensive field experiments have been made in the airshed, it is not possible to accurately characterize the second component of the dry deposition process. An alternative approach, and the focus of this work, is to develop an upper limit for v_g in terms of the transport processes, and the concentration at a reference point above the surface. (Typically the height of the lowest computational grid point in the airshed model.) A secondary goal is to identify the significant meteorological variables and surface properties needed to either correlate different measurements of v_g or to modify the results for different experimental conditions.

IV. DEPOSITION IN THE CONSTANT FLUX LAYER

Consider the idealized representation of the airshed surface shown in Figure 3. Within the layer $0 \leq z \leq z_r$ the deposition is assumed to be a one-dimensional, steady state, constant flux process occurring without re-entrainment and, in the case of aerosols, without particle agglomeration. With these assumptions the deposition flux is described by

$$F = [K_p(z) + D] \frac{dc}{dz} + v_t \, c(z) \qquad (6)$$

where $K_p(z)$ is the pollutant eddy diffusion coefficient, D the molecular diffusion coefficient of the material in air and v_t the terminal settling velocity for particulate material. Equating the fluxes in

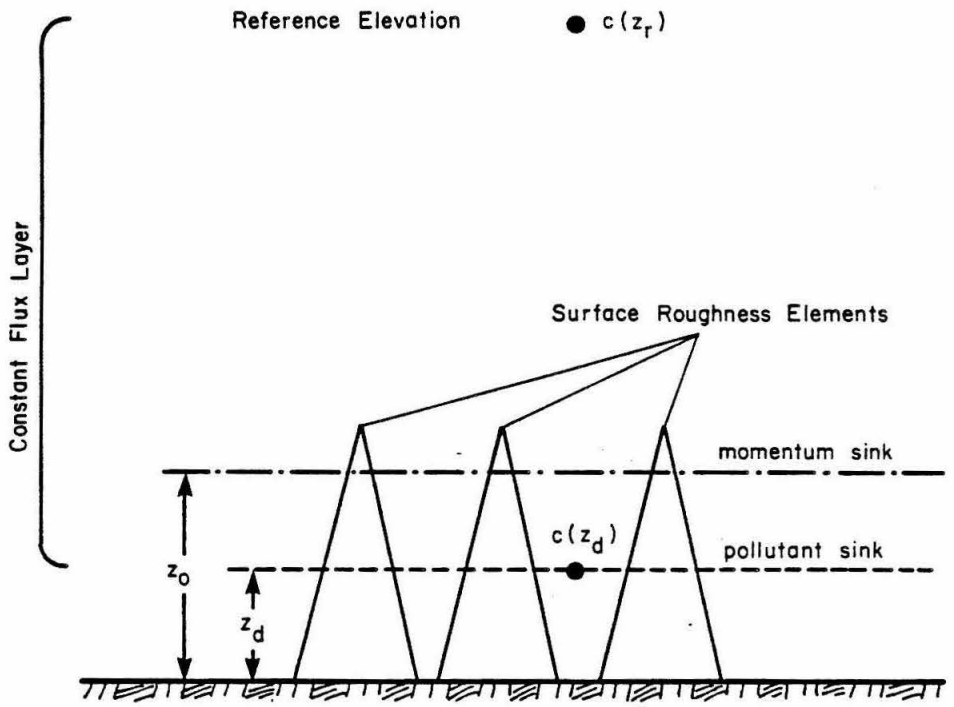

FIGURE 3

Idealized Representation of the Airshed Surface

expressions (5) and (6) gives

$$\int_{z_d}^{z_r} \frac{dz}{[K_p(z)+D]} = \int_{c(z_d)}^{c(z_r)} \frac{dc}{[v_g c(z_r) - v_t c(z)]} \qquad (7)$$

The lower limits of integration z_d and $c(z_d)$ refer to the elevation and concentration of material at the effective pollutant sink height. It is important to note that z_d is not in general equal to the surface roughness z_o, a height associated with momentum sink[26]. If the terminal settling velocity is set to zero for the case of gaseous materials then (7) can be written in the simpler form

$$v_g = \frac{\left[1 - \frac{c(z_d)}{c(z_r)} \right]}{\int_{z_d}^{z_r} \frac{dz}{[K_p(z) + D]}} \qquad (8)$$

V. DIFFUSIVE TRANSPORT IN THE SURFACE LAYER

Since the model is intended to be used primarily in the surface layer of the atmosphere, an expression for $K_p(z)$ can be developed using Monin-Obukhov similarity theory. The velocity shear and the pollutant eddy diffusion coefficient, $K_p(z)$, are given by

$$\frac{\partial u}{\partial z} = \frac{u_*}{kz} \phi_m\left(\frac{z}{L}\right) \qquad (9)$$

and

$$K_p(z) = \frac{k\, u_*\, z}{\phi_p\left(\frac{z}{L}\right)} \qquad (10)$$

where k is the von Karman constant, u_* the friction velocity, L the Monin-Obukhov length and ϕ_p, ϕ_m are universal functions which must be determined by experiment. The ϕ functions basically correct for the effects of buoyancy on turbulence. Businger et al.[27] have constructed

expressions for momentum, ϕ_m, and heat, ϕ_H, from an analysis of field data taken under a wide variety of stability conditions. For the present model the expressions adopted for momentum are

$$\phi_m\left(\frac{z}{L}\right) = \begin{cases} \left[1 + 4.7\left(\frac{z}{L}\right)\right] & \text{Stable; } \frac{z}{L} > 0 \\ 1 & \text{Neutral; } \frac{z}{L} = 0 \\ \left[1 - 15\left(\frac{z}{L}\right)\right]^{-\frac{1}{4}} & \text{Unstable: } \frac{z}{L} < 0 \end{cases} \tag{11}$$

In addition to the transport relations for momentum there are some data for ϕ functions associated with water vapor ϕ_w and heat ϕ_H. Unfortunately, there are few direct experimental measurements of pollutant fluxes in the atmospheric surface layer.

A decision must be made as to the form of the ϕ function for a generalized passive scalar contaminant. For unstable conditions ($z/L < 0$) the experimental evidence of Dyer and Hicks[28] indicates that ϕ_H, $\phi_w = \phi_m^2$. Galbally[29] measured ozone profiles and fluxes in the surface layer and concluded that the eddy transport mechanism for O_3 is similar to that for heat rather than momentum. On the basis of these two studies and the data of Businger et al.[27] the following ϕ functions have been adopted for pollutant transport.

$$\phi_p\left(\frac{z}{L}\right) = \begin{cases} 0.74 + 4.7\left(\frac{z}{L}\right) & \text{Stable; } \frac{z}{L} > 0 \\ 0.74 & \text{Neutral; } \frac{z}{L} = 0 \\ 0.74\left[1 - 9\left(\frac{z}{L}\right)\right]^{-\frac{1}{2}} & \text{Unstable; } \frac{z}{L} < 0 \end{cases} \tag{12}$$

VI. UPPER LIMIT DEPOSITION MODEL

Within the surface layer defined by $z_d<z<z_r$ the bulk contribution to the diffusive transport from molecular diffusion is negligible. Applying this assumption to equation (8) and in addition substituting the flux gradient relation (10) for $K_p(z)$ gives the following upper limit to the deposition velocity.

$$v_g = \frac{k\left[1 - \frac{c(z_d)}{c(z_r)}\right]}{\int_{z_d}^{z_r} \frac{1}{zu_*}\,\phi_p(\frac{z}{L})\,dz} \tag{13}$$

Since u_* is approximately constant with height in the surface layer[30] and $\phi_p \sim 1$ for $z_d<z<z_o$, the denominator of (13) can be expanded to give

$$v_g = \frac{k^2\, u(z_r)\left[1 - \frac{c(z_d)}{c(z_r)}\right]}{\left[\int_{z_o}^{z_r} \phi_m(\frac{z}{L})\,\frac{dz}{z}\right]\left[\ell n(\frac{z_o}{z_d}) + \int_{z_o}^{z_r} \phi_p(\frac{z}{L})\,\frac{dz}{z}\right]} \tag{14}$$

Evaluation of the term $\ln(z_o/z_d)$ in the denominator of equation (14) requires a knowledge of z_d and of the transfer processes at the surface. Based on a survey of the heat transfer literature Wesely and Hicks[31] assumed that

$$\ell n\left(\frac{z_o}{z_d}\right) = 2(\frac{Sc}{Pr})^{\frac{2}{3}} \tag{15}$$

where Sc and Pr are the Schmidt and Prandtl numbers associated with

the pollutant material in air. The complete model is then

$$v_g = \frac{k^2\, u(z_r)\left[1-\frac{c(z_d)}{c(z_r)}\right]}{\left[\int_{z_o}^{z_r} \phi_m(\frac{z}{L})\,\frac{dz}{z}\right]\left[2(\frac{Sc}{Pr})^{\frac{2}{3}} + \int_{z_o}^{z_r} \phi_p(\frac{z}{L})\,\frac{dz}{z}\right]} \qquad (16)$$

The integrals required to evaluate v_g are shown in Table 1.

VII. CHARACTERISTICS OF THE DEPOSITION MODEL

The final result exposes a number of the limitations of the basic model (5), in particular, the fact that v_g is directly influenced by the prevailing meteorology and atmospheric stability. The effect of stability is particularly apparent; consider for example, the conditions shown in Figure 4. With z/L in the range -1.5 to +1.5, the deposition velocities vary by almost a factor of five. This result indicates that under typical conditions there could be a significant diurnal variation in the surface removal of pollutant material. The functional dependence of v_g on the elevation above the surface highlights the need for reporting the reference height z_r in field or laboratory studies. If v_g, z_r, z_o and $u(z_r)$ are measured, then it is possible to evaluate $c(z_d)/c(z_r)$ and in turn, v_g for elevations other than the reference height. This is a useful approach for developing the deposition velocities for air quality models in which z_r may be of O(10 m).

Once the pollutant deposition velocity has been established, either by direct measurement or estimated using the proposed model, the next step is to develop a formal procedure for calculating the amount of material removed at the ground. At the lower surface of the airshed

TABLE 1

Momentum and Pollutant Integrals for Different Stability Conditions

INTEGRAL	STABILITY CONDITION		
	STABLE	NEUTRAL	UNSTABLE
	$\frac{z}{L} > 0$	$\frac{z}{L} = 0$	$\frac{z}{L} < 0$
MOMENTUM $\int_{z_o}^{z_r} \phi_m(\frac{z}{L}) \frac{dz}{z}$	$\ln(\frac{z_r}{z_o}) + \frac{4.7}{L}(z_r - z_o)$	$\ln(\frac{z_r}{z_o})$	$\ln\left[\frac{(1-15\frac{z_r}{L})^{\frac{1}{4}} - 1}{(1-15\frac{z_r}{L})^{\frac{1}{4}} + 1}\right] - \ln\left[\frac{(1-15\frac{z_o}{L})^{\frac{1}{4}} - 1}{(1-15\frac{z_o}{L})^{\frac{1}{4}} + 1}\right] + 2\arctan(1-15\frac{z_r}{L})^{\frac{1}{4}} - 2\arctan(1-15\frac{z_o}{L})^{\frac{1}{4}}$
POLLUTANT $\int_{z_o}^{z_r} \phi_p(\frac{z}{L}) \frac{dz}{z}$	$0.74\ln(\frac{z_r}{z_o}) + \frac{4.7}{L}(z_r - z_o)$	$0.74\ln(\frac{z_r}{z_o})$	$0.74\left\{\ln\left[\frac{(1-9\frac{z_r}{L})^{\frac{1}{2}} - 1}{(1-9\frac{z_r}{L})^{\frac{1}{2}} + 1}\right] - \ln\left[\frac{(1-9\frac{z_o}{L})^{\frac{1}{2}} - 1}{(1-9\frac{z_o}{L})^{\frac{1}{2}} + 1}\right]\right\}$
DEPOSITION $\int_{z_r}^{\Delta z}\int_{z_r}^{z} \phi_p(\frac{x}{L}) \frac{dx}{x} dz$	$0.74(\Delta z \ \ell n \frac{\Delta z}{z_r} - \Delta z + z_r) + \frac{2.35}{L}(\Delta z - z_r)^2$	$0.74(\Delta z \ \ell n \frac{\Delta z}{z_r} - \Delta z + z_r)$	$0.74\ \Delta z\ \ell n\left[\left(\frac{\sqrt{1-9\frac{\Delta z}{L}} - 1}{\sqrt{1-9\frac{z_r}{L}} - 1}\right)\left(\frac{\sqrt{1-9\frac{z_r}{L}} + 1}{\sqrt{1-9\frac{\Delta z}{L}} + 1}\right)\right] + 0.104\ L\left[\sqrt{1-9\frac{\Delta z}{L}} - \sqrt{1-9\frac{z_r}{L}}\right]$

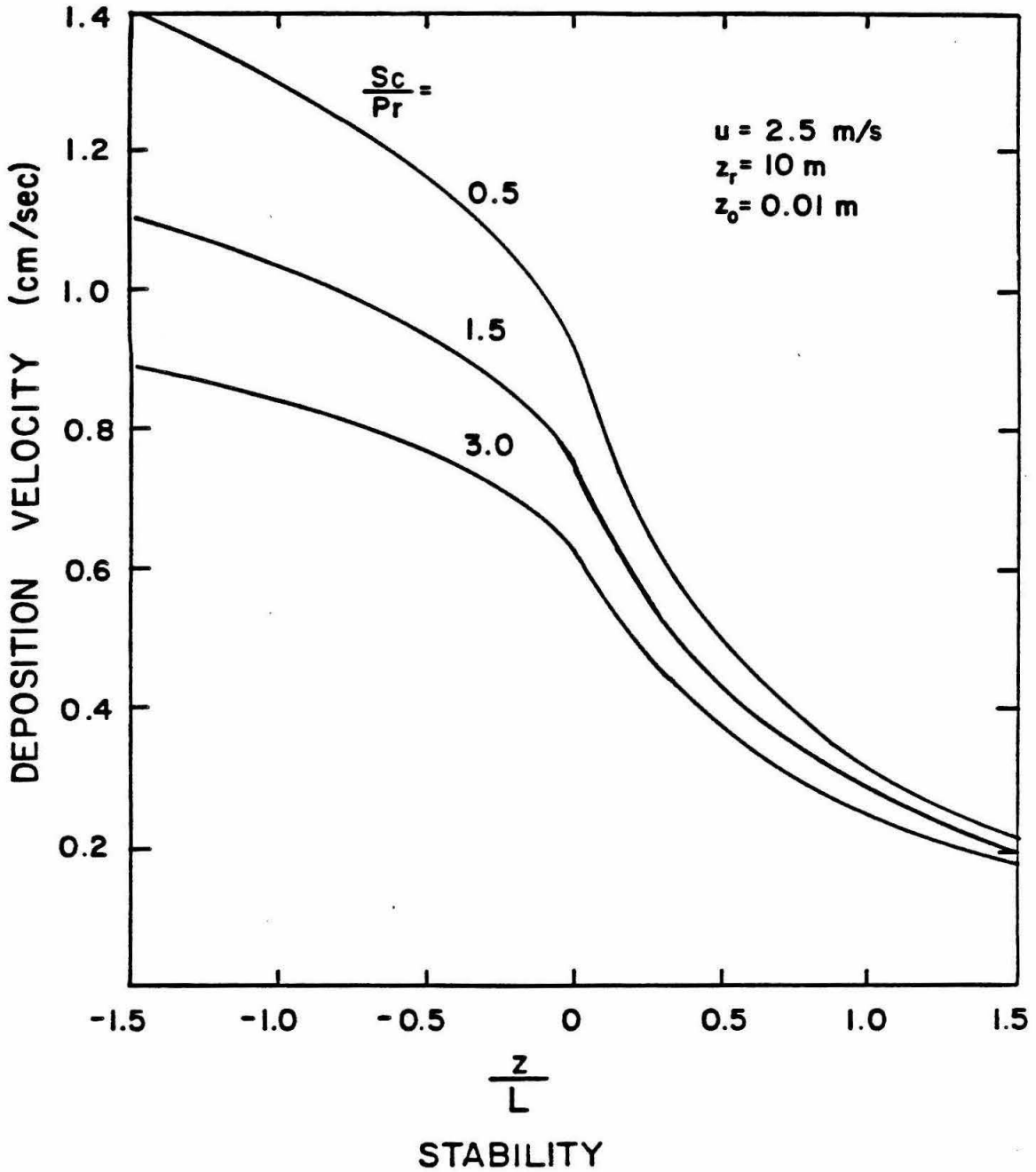

FIGURE 4

Variation of Surface Deposition Velocity as a Function of Atmospheric Stability and Sc/Pr Ratio ($c(z_d)/d(z_r)=0$)

the pollutant removal is typically described by the boundary condition:

$$F \equiv - K_p(z) \left.\frac{\partial c}{\partial z}\right|_{z = z_r} = - v_g(z_r)\, c(z_r) \qquad (17)$$

Where z_r is a reference elevation, $v_g(z_r)$ and $c(z_r)$ are the pollutant deposition velocity and concentration at that height Because of the nonlinear nature of $K_p(z)$, most mathematical descriptions of pollutant transport require numerical solution. This can pose a problem in that the elevation of the lowest computation grid point is typically much higher than the reference height, z_r, used to establish the pollutant deposition velocities. The situation is illustrated in Figure 5 where z is the height, z_r, used to establish the pollutant deposition velocities. Because of the need to approximate the vertical concentration profile in discrete increments $c(z_r)$ is not readily available. When coupled with the observation that v_g varies with height there is a need to develop an equivalent deposition velocity v_g that, when applied to the cell average concentration, c_1, correctly predicts the flux at the lower boundary. One way to develop such a model is to assume that most of the lowest cell is within the surface or constant flux layer. If this is the case then the cell deposition velocity is given by

$$\bar{v}_g = \frac{v_g(z_r)c(z_r)}{c_1} \qquad (18)$$

If c_1 is to represent the average value of the actual vertical concentration distribution in the range $z_r < z < \Delta z$ then it must be equivalent to

$$c_1 = \frac{1}{\Delta z - z_r} \int_{z_r}^{\Delta z} c(z)dz \qquad (19)$$

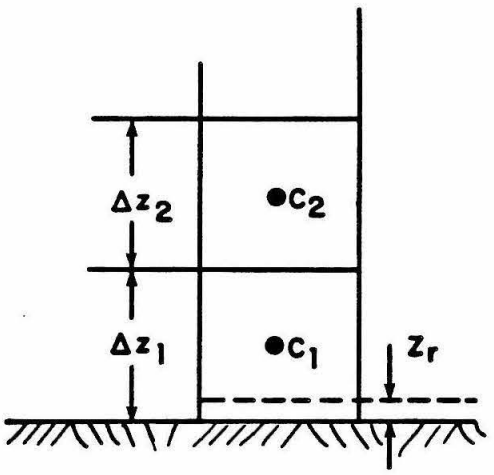

(a)

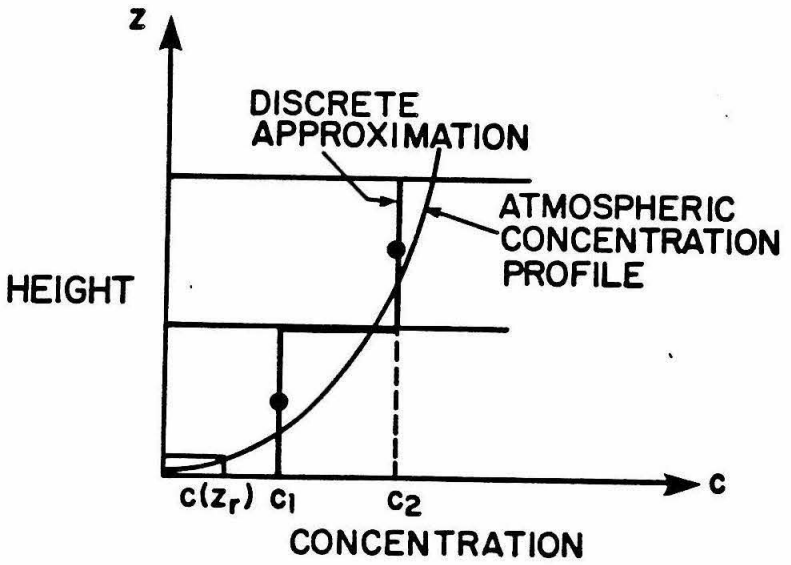

(b)

FIGURE 5

Nomenclature for cell-average deposition model
(a) computational grid
(b) discrete approximation of vertical concentration profile

Within the constant flux layer c(z) is given by

$$c(z) = c(z_r) \left[1 + v_g(z_r) \int_{z_r}^{z} \frac{1}{K_p(z)} \, dz \right] \tag{20}$$

The equivalent cell deposition velocity can now be determined by combining (20), (19), (18) and (10) to give

$$\overline{v}_g = \frac{v_g(z_r)}{1 + \frac{v_g(z_r)}{ku_*(\Delta z - z_r)} \int_{z_r}^{\Delta z} \int_{z_r}^{z} \phi_p(\frac{x}{L}) \frac{dx}{x} \, dz} \tag{21}$$

The integrals needed to evaluate the denominator of (17) are shown in Table 1. An example of the variation of v_g with cell size and atmospheric stability is shown in Figure 6, and as can be expected, the equivalent deposition velocity becomes smaller as Δz increases. The variation is most pronounced under stable conditions because of the reduced vertical mixing. One implication of this result is that if $v_g(z_r)$, rather than v_g, were to be used in a practical calculation then the surface removal flux would be considerably overestimated.

VIII. EXPERIMENTAL METHODS FOR DETERMINING DEPOSITION VELOCITIES

In the previous section primary attention was directed at developing an upper limit estimate of the rate at which pollutants can be transported to the ground. Whether this flux corresponds to the actual removal rate depends to a large extent on the conditions and type of the underlying surface. Garland[32], for example, has observed an order of magnitude difference in the ozone (O_3) deposition velocity over different soil types. If $c(z_d)$ is the pollutant concentration at

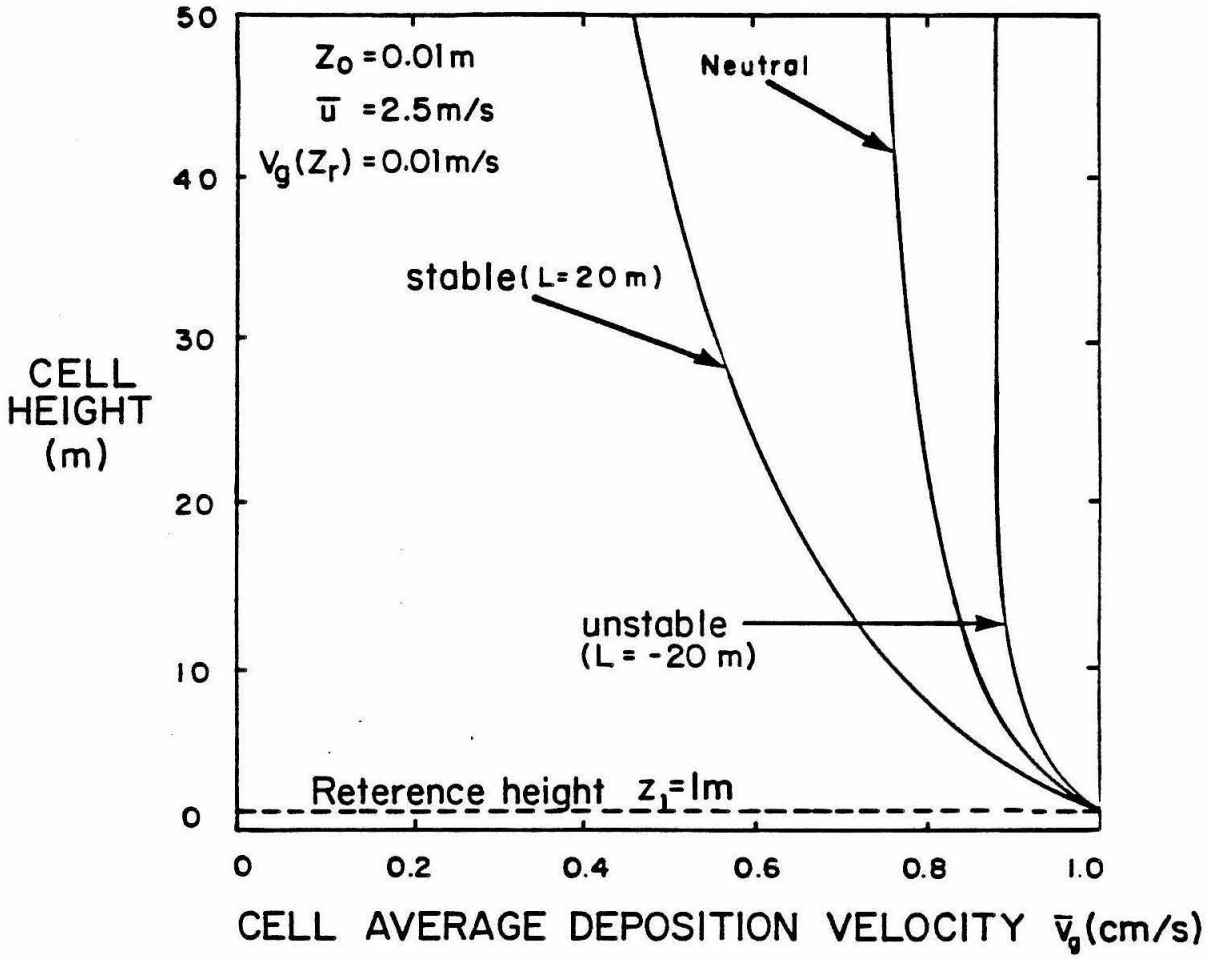

FIGURE 6

Variation of Average Deposition Velocity as a Function of Atmospheric Stability and Computational Cell Height ($c(z_d)/c(z_r)=0$)

the effective sink height, z_d, then the upper and lower limits on v_g correspond to the conditions $c(z_d) = 0$ and $c(z_r) = c(z_d)$. If a lower bound on v_g is required then it is important to be able to estimate the concentration difference $c(z_r) - c(z_d)$. At present the only satisfactory means for establishing the surface condition is by experimental measurement. This section presents a brief survey of field and laboratory techniques for determining deposition velocities for gaseous species which participate in photochemical reaction processes.

Whether pollutant deposition velocities are measured in the field or under laboratory conditions usually one of several basic techniques is employed. Three of the most common are: the use of radioactive tracers, free stream concentration decay measurements and gradient or profile determinations. The most widely used laboratory procedure is called the flux method which equates free stream concentrations decay rates to the surface removal fluxes. Garland and Penkett[33] measured the concentration decay of peroxy acetyl nitrate (PAN) as it passed over different surfaces in a wind tunnel. Given the concentration difference, the travel time over the surface and the wind tunnel dimensions it is a simple task to infer the net deposition flux and in turn determine the deposition velocity. A similar technique as used by Hill and Chamberlain[17] to establish the pollutant influx required to maintain a constant concentration over different plant canopies. More recently the emergence of fast response pollutant detectors has enabled a direct measurement of the vertical turbulent flux. Wesely et al.[34-36] recorded the velocity, w', and concentration, c', fluctuations at a

reference height of $z_r = 5$ and evaluated v_g directly using

$$v_g(z_r) = \left. \frac{\overline{w'c'}}{\bar{c}} \right|_{z = z_r} \qquad (22)$$

where $\overline{w'c'}$ is the time averaged vertical turbulent flux and $\bar{c}$ the average concentration. The averaging time for the results reported in Wesely et al.[34] was O(10 minutes).

Another means for determining deposition velocities is to employ isotopic labelling techniques. If isotopes, with low natural abundances, are used then the task of differentiating between material previously present at the surface and the amount deposited during the experiment is considerably simplified. Owens and Powell[37] released sulfur dioxide (SO_2), labelled with the sulfur isotope ${}_{16}S^{35}$, and measured the accumulation of $^{35}SO_2$ at the ground. Given the exposure time, T, and the $^{35}SO_2$ concentration at the reference elevation the deposition velocity is given by

$$v_g(z_r) = \frac{^{35}SO_2 \text{ Activity at the Ground}}{T \quad ^{35}SO_2(z_r)} \qquad (23)$$

Chamberlain[16] used thorium-B (${}_{82}Pb^{212}$), in a wind tunnel, to measure the vertical flux of pollutant materials towards grass and similar surfaces as a function of the concentration difference between the reference height and the surface.

The most common technique used in field studies is the gradient or profile method. This procedure utilizes measurements at two or more elevations to establish the vertical concentration gradient $\partial c/\partial z$. If the momentum, heat, water vapor, and pollutant fluxes are constant

within the surface layer then the Monin-Obukhov similarity hypothesis, coupled with the measured vertical gradient, gives the pollutant deposition velocity.

$$v_g(z_r) = \left. \frac{K_p(z)}{c(z)} \frac{\partial c}{\partial z} \right|_{z = z_r} \tag{24}$$

The turbulent eddy diffusivity $K_p(z)$ can be estimated using the methods presented above or determined from energy budget measurements using a mass transfer analogy. An alternative approach is to assume that the pollutant transport is similar to that of water vapor and employ a stability dependent bulk transfer coefficient to approximate the surface flux. Given the measured concentration profile the deposition velocity is simply

$$v_g(z_r) = C\bar{u}(z_h) \left(\frac{c(z_h) - c(z_d)}{c(z_r) - c(z_d)} \right) \tag{25}$$

where C is the aerodynamic transfer coefficient and $\bar{u}(z_h)$ is the mean wind speed at an elevation z_h above the ground. Whelpdale and Shaw[38] used (25) to evaluate (SO_2) deposition velocities over different surfaces.

IX. LITERATURE SURVEY OF DEPOSITION VELOCITY MEASUREMENTS

A major goal of developing the upper limit deposition model was to establish the surface removal rates for those species which participate in photochemical reactions. A partial list of these species includes nitric oxide (NO), nitrogen dioxide (NO_2), ozone (O_3), peroxy acetyl nitrate (PAN), hydrogen peroxide (H_2O_2), nitrous acid (HONO), nitric acid (HNO_3) carbon monoxide (CO), reactive hydrocarbons, organic and

inorganic radicals. An extensive literature search was carried out to identify experimental determinations of ground level deposition velocities for each of these species. The results, presented in Table 2, include additional values excerpted from the comprehensive surveys conducted by Droppo[39], Slinn et al.[40] and McMahon and Denison[22]. In constructing the table an attempt has been made to summarize those factors which influence the estimates namely the experimental technique, reference height, type of surface, moisture conditions and the atmospheric conditions.

Considering the important role of deposition in establishing ambient concentration levels the most striking feature of Table 2 is the paucity of reported results. For example, during the literature survey no field measurements were found for particulate nitrates, ammonia (NH_3) or nitric acid (HNO_3). This problem is further compounded by inadequate documentation of the atmospheric conditions prevailing during each of the experiments. Unless sufficient meteorological data are reported it is difficult to separate whether the turbulent transport or chemical nature of the underlying surface is controlling the deposition.

The limited data reported in the Table 3 are, unfortunately, insufficient to adequately verify the quantitative performance of the upper limit model. A qualitative indication can, however, be gained by examining the sulfur dioxide (SO_2) deposition study of Whelpdale and Shaw[38] and the ozone (O_3) and nitrogen dioxide (NO_2) fluxes measured by Wesely et al.[34-36] In each case the reported influence of atmospheric stability is consistent with the calculated variations shown in

TABLE 2

Literature Survey of Deposition Velocity Data for Species Involved in Photochemical Reaction Processes

SPECIES	DEPOSITION VELOCITY v_g(cm/s)	SURFACE CONDITIONS	MEASUREMENT METHOD	METEOROLOGICAL DATA REPORTED	REFERENCE
O_3	1.67	Alfalfa	Flux	$\bar{u}$	Hill and Chamberlain[17]
	0.10-2.10	Soil, Short Grass	Profile	$z/L, R_{ib}, u_*, z_r$=4m, T, RH, z_o	Galbally[29]
	0.47-0.55	Grass, Soil, Water	Flux	$\bar{u}, u_*, z_o, z_r$=10cm	Garland and Penkett[33]
	0.20-0.80	Maize	Flux	$\bar{u}, u_*, z_o$, w, T, z_r=4-5m	Wesely et al.[35]
	0.60-6.30	---	---	---	Droppo[39]
	0.02-1.80	---	---	---	McMahon and Denison[22]
	0.29-0.84	Soybean Field	Eddy-correlation	$\bar{u}, z_r$=5.2m, L	Wesley et al.[36]
NO	0.10	Alfalfa	Flux	$\bar{u}$	Hill and Chamberlain[17]
	0.10-0.20	Soil, Cement	---	---	Judeikis and Wren[41]
	0.10	---	---	calculated	Sehmel[23]
NO_2	1.90	Alfalfa	Flux	$\bar{u}$	Hill and Chamberlain[17]
	0.50-2.00	---	---	---	McMahon and Denison[22]
	0.05-56	Soybean Field	Eddy-correlation	$\bar{u}, z_r$=5.2m, L	Wesley et al.[36]
	0.30-0.80	Soil, Cement	---	---	Judeikis and Wren[41]
PAN	0.14-0.30	Grass, Soil	Flux	$\bar{u}, u_*, z_o, z_r$=10 cm	Garland and Penkett[33]
	0.63	Alfalfa	Flux	$\bar{u}$	Hill and Chamberlain[17]
	0.80	Alfalfa	---	calculated	Sehmel[23]

TABLE 3

Summary of Deposition Velocity Concentration Ratios[a]

SPECIES	CONCENTRATION RATIO $\left[1 - \frac{c(z_d)}{c(z_r)}\right]$
CO	0.0
NO	0.1
NH_4NO_3	0.2
PAN	0.25
NO_2	0.6
O_3	0.8
NH_3	0.8
HNO_3	0.8

[a]Based on a reference elevation z_r = 1 m.

Figure 4. During stable conditions the deposition flux is primarily controlled by the rate at which material can be transported to the surface. Such circumstances are likely to occur at night. During the daytime however, the deposition rate is much more likely to be influenced by chemical interactions at the surface. For example, the uptake by vegetation can be expected to much greater because the leaf stoma are likely to be open. One obvious conclusion from this discussion is that there is a great need for additional field measurements that can characterize the influence of surface chemistry. Given these caveats, Table 3 summarizes the concentration ratios used in (16). The values for ammonia and nitric acid were estimated by assuming that their chemical reactivity and solubility were similar to that of sulfur dioxide or ozone.

X. EVALUATION OF THE DEPOSITION MODEL

In the previous sections a simple upper limit model for estimating deposition velocities has been presented. The principal features of the formulation are: an explicit treatment of atmospheric stability and a formal procedure for determining equivalent cell average deposition velocities for use in numerical calculations. The fact that atmospheric stability has such a pronounced effect on the surface fluxes points to the need for careful reporting of meteorological conditions during field studies. This would enable an independent assessment of whether the limits on v_g are set by the eddy diffusion or by the ability of the underlying surface to assimilate the material. In terms of future work considerably more attention needs to be given to characterizing the physical and chemical processes occurring in the

layer $z_d < z < z_o$. At present there are no satisfactory theoretical treatments of the mass transfer close to the surface. Even more serious is the limited amount of field data on pollutant uptake at the surface.

A basic limitation of the model is its reliance on Monin-Obukhov similarity theory to characterize the material fluxes in the surface layer. While this formally restricts applications to steady conditions and values $|z/L| < 1$, the model is, nevertheless, capable of producing useful limits for surface deposition fluxes for a range of the species encountered in photochemical modeling applications.

XI. PHOTOCHEMISTRY OF NITROGEN OXIDES

In the polluted troposphere the chemistry of nitrogen containing species rivals that of sulfur both interms of the range of compounds present as well as their impact on acid deposition. Nitrogen oxides (NO_x) emissions and their oxidation products have long been recognized as a source for acidic materials in the atmosphere. Based on a series of field experiments conducted in the early 1820's Lavoisier concluded that nitric acid deposited at the ground had its origin in the air.[42] There are several reasons why NO_x emissions are important. One is that nitric ($HONO_2$) and nitrous (HONO) acids can be formed by direct oxidation of nitric oxide (NO), the dominant component of NO_x emissions. In addition, emissions of nitrogen oxides act as essential precursors to the formation of strong oxidants such as hydrogen peroxide and ozone.

In an urban atmosphere the major observed features of the chemical interaction between hydrocarbons and NO_x are: the conversion of NO to NO_2, the accumulation of ozone (O_3), the production of nitric acid and

the generation of organic nitrates. While there are a number of alternative ways of modeling the chemical kinetics of this system the approach used in this work is based on the work of Falls and Seinfeld[11], Falls et al.[12] and McRae et al.[5,6] The mechanism, shown in Table 4, is composed of 52 reaction steps and is designed to describe the concentration dynamics of thirty two different species. The major nitrogen containing compounds are listed in Table 5. One measure of the chemical diversity of these species is that the nitrogen oxidation states vary from -3 for ammonia (NH_3) to +5 for peroxynitric acid (HO_2NO_2). (The kinetic data needed to specify the reaction rate constants are discussed in the references [5-6,43-53].) This particular mechanism was selected because it incorporates recent information on rate constants, mechanistic structure and, in addition, its performance has been successfully tested against smog chamber experiments. One other reason for choosing this scheme is that it compatible with the emissions inventory data available in the South Coast Air Basin.

In this work primary attention is directed at the fate and end products of nitrogen oxide emissions. For this reason it is useful to be able to follow the flow of nitrogen through the chemical mechanism and account for the various sources and sinks. A schematic representation of the interactions between nitrogen containing compounds is shown in Figure 7. Besides the direct emissions of nitric oxide (NO), some of the other more abundant nitrogenous species, produced by the photochemical reactions, are nitric acid ($HONO_2$), nitrogen dioxide (NO_2) and peroxyacetyl nitrate (PAN). Nitric acid is particularly important because of its contribution to acid deposition and the fact that it acts as a precursor for the formation of ammonium nitrate aerosol.

TABLE 4

Photochemical Reaction Mechanism

REACTION STEP					RATE CONSTANT (ppm-min units)		VALUE AT 298 ^{o}K	REF[a] (NOTES)
NO_2	+ hv	$\xrightarrow{1}$	NO	+ $O(^3P)$			0.51	(b)
$O(^3P)$	+ O_2 + M	$\xrightarrow{2}$	O_3	+ M	$\frac{0.346}{T^2}$	exp(510/T)	2.16×10^{-5}	[1]
O_3	+ NO	$\xrightarrow{3}$	NO_2	+ O_2	$\frac{9.24\times10^5}{T}$	exp(-1450/T)	2.39×10^{1}	[1]
NO_2	+ $O(^3P)$	$\xrightarrow{4}$	NO	+ O_2	$\frac{3.99\times10^6}{T}$		1.34×10^{4}	[1]
NO	+ $O(^3P)$	$\xrightarrow{5}$	NO_2		$\frac{1.67\times10^5}{T}$	exp(584/T)	3.98×10^{3}	[1]
NO_2	+ $O(^3P)$	$\xrightarrow{6}$	NO_3		$\frac{1.07\times10^6}{T}$		3.59×10^{3}	[1]
O_3	+ NO_2	$\xrightarrow{7}$	NO_3	+ O_2	$\frac{5.19\times10^4}{T}$	exp(-2450/T)	4.68×10^{-2}	[1]
NO_3	+ NO	$\xrightarrow{8}$	$2NO_2$		$\frac{8.05\times10^6}{T}$		2.70×10^{4}	[2]
NO	+ OH	$\xrightarrow{9}$	HONO		$\frac{5.07\times10^6}{T}$		1.70×10^{4}	[1]
HONO	+ hv	$\xrightarrow{10}$	OH	+ NO			0.096	(b)
HO_2	+ NO_2	$\xrightarrow{11}$	HONO	+ O_2	$k_{11} = 0.001\ k_{13}$		1.70	[3]
HONO	+ OH	$\xrightarrow{12}$	NO_2	+ H_2O	$\frac{2.91\times10^6}{T}$		9.77×10^{3}	[1]

TABLE 4 (Cont)

REACTION STEP				RATE CONSTANT (ppm-min units)		VALUE AT 298 °K	
NO_2	+ HO_2	13 →	HO_2NO_2	$\frac{1.73\times10^4}{T}$	exp(1006/T)	1.70×10^3	[4]
HO_2NO_2		14 →	HO_2 + NO_2	1.80×10^{15}	exp(-9950/T)	5.68	[4]
HO_2	+ NO	15 →	NO_2 + OH	$\frac{3.58\times10^6}{T}$		1.20×10^4	[1]
RO_2	+ NO	16 →	NO_2 + RO	$\frac{3.58\times10^6}{T}$		1.20×10^4	[5]
RCO_3	+ NO	17 →	NO_2+RO_2+CO_2	$\frac{1.13\times10^6}{T}$		3.79×10^3	[6]
NO_2	+ OH	18 →	$HONO_2$	$\frac{4.53\times10^6}{T}$		1.52×10^4	[1]
CO	+ OH	19 →	HO_2 + CO_2	$\frac{1.31\times10^5}{T}$		4.40×10^2	[1]
O_3	+ hv	20 →	$O(^3P)$ + O_2			0.0328	(b)
HCHO	+ hv	21 →	$2HO_2$ + CO			0.00284	(b)
HCHO	+ hv	22 →	H_2 + CO			0.00473	(b)
HCHO	+ OH	23 →	HO_2+H_2O+CO			1.39×10^4	(c)
RCHO	+ hv	24 →	RO_2+HO_2+CO			0.0026	(c)
RCHO	+ OH	25 →	RCO_3			2.57×10^4	(c)

TABLE 4 (Cont)

REACTION STEP				RATE CONSTANT (ppm-min units)	VALUE AT 298 °K	
C_2H_4	+ OH	26 →	RO_2		1.16×10^4	(c)
C_2H_4	+ $O(^3P)$	27 →	RO_2 + HO_2		1.22×10^3	(c)
OLE	+ OH	28 →	RO_2		8.91×10^4	(c)
OLE	+ $O(^3P)$	29 →	RO_2 + RCO_3		2.21×10^4	(c)
OLE	+ O_3	30 →	(a_1)RCHO + (a_2)HCHO + $(a_3)HO_2$ + $(a_4)RO_2$ + (a_5)OH + $(a_6)RO^2$		0.136	(c)
ALK	+ OH	31 →	RO_2		4.7×10^3	(c)
ALK	+ $O(^3P)$	32 →	RO_2 + OH		99.8	(c)
ARO	+ OH	33 →	RO_2 + RCHO		1.61×10^4	(c)
RO		34 →	$(b_1)HO_2$ + (b_2)HCHO + (b_3)RCHO + $(1-b_1)$ RO_2		2.0×10^5	[7]
RONO	+ hv	35 →	NO + RO		0.112	(d)
RO	+ NO	36 →	RONO	$\frac{4.38 \times 10^6}{T}$	1.47×10^4	[8]
RO	+ NO_2	37 →	$RONO_2$	$\frac{2.19 \times 10^6}{T}$	7.35×10^3	[8]
RO	+ NO_2	38 →	RCHO + HONO	$k_{38}=0.087\ k_{37}$	6.39×10^2	[9](e)

TABLE 4 (Cont)

REACTION STEP					RATE CONSTANT (ppm-min units)		VALUE AT 298 °K	
NO_2	+ RO_2	39 →	RO_2NO_2		$\frac{1.64\times10^{6}}{T}$		5.50×10^{3}	[10](f)
NO_2	+ RO_2	40 →	RCHO	+ $HONO_2$	$\frac{1.64\times10^{3}}{T}$		5.50	[10]
RO_2NO_2		41 →	NO_2	+ RO_2	same as k_{14}		5.68	[5]
RCO_3	+ NO_2	42 →	PAN		$\frac{6.17\times10^{5}}{T}$		2.07×10^{3}	[6]
PAN		43 →	RCO_3	+ NO_2	4.77×10^{16}	exp(-12516/T)	2.74×10^{-2}	[6]
NO_2	+ NO_3	44 →	N_2O_5		$\frac{2.20\times10^{6}}{T}$		7.39×10^{3}	[13]
N_2O_5		45 →	NO_2	+ NO_3	3.44×10^{16}	exp(-10600/T)	1.22×10^{1}	[13]
H_2O	+ N_2O_5	46 →	$2HONO_2$		$\frac{4.47\times10^{-3}}{T}$		1.50×10^{-5}	[1]
O_3	+ OH	47 →	HO_2	+ O_2	$\frac{6.62\times10^{5}}{T}$	exp(-1000/T)	7.75×10^{1}	[1]
O_3	+ HO_2	48 →	OH	+ $2O_2$	$\frac{4.85\times10^{3}}{T}$	exp(-580/T)	2.32	[11]
O_3		49 →	wall loss		0.0	Depends on the experiment		(g)

TABLE 4 (Cont)

REACTION STEP					RATE CONSTANT (ppm-min units)		VALUE AT 298 °K	
HO_2	+ HO_2	50 →	H_2O_2	+ O_2	$\frac{3.4\times10^{4}}{T}$ exp(1100/T)+ $\frac{5.8\times10^{-5}}{T^2}$ exp(5800/T)[H20]		8.28×10^{3}	[11](i)
H_2O_2	+ hv	51 →	2OH				1.61×10^{-3}	
RO_2	+ RO_2	52 →	2RO		$\frac{2.04\times10^{4}}{T}$	exp(223/T)	1.45×10^{2}	[12]

Footnotes:

a)
[1] Hampson and Garvin[43]
[2] Graham and Johnston[44]
[3] Graham et al.[45]
[4] Graham et al.[45]
[5] Estimate
[6] Cox and Roffey[46]
[7] Baldwin et al.[47]
[8] Batt and Rattray[48]
[9] Baker and Shaw[49]
[10] Simonaitis and Heicklen[50]
[11] NASA[51]
[12] Sander and Watson[52]
[13] Baulch et al.[53]

b) All values are for Los Angeles California (latitude 34.06°, longitude 118.25°, time zone = 8.0). The rates are the peaks values that occured at 12:00 Pacific Standard Time, 26 June 1974.

c) Lumped hydrocarbon reaction rates are based on the individual species rates weighted on a molar basis in terms of their contribution to the emissions inventory for SCAB.

d) Photolysis rate set to 0.22 of NO_2.

e) $k_{47}/(k_{37} + k_{38}) = 0.92$ for CH_3, $k_{38} = 0.087\ k_{37}$

TABLE 4 (Cont)

f) Rate constants for reactions 39 and 40 are based on the assumption that $k_{16}/(k_{39} + k_{40}) = 2.2$.

g) Wall loss term for modeling smog chamber experiments, k_{49} depends on experimental conditions.

h) Determined from $1.477 \times 10^{15} \times 10^{-(11.6T/(17.4 + T))} \sqrt{(280/T)}$

i) Water concentration in ppm, value at $298^{o}K$ based on 2,000 ppm.

TABLE 5

Some Important Nitrogen-Containing Species

SPECIES	CHEMICAL SYMBOL	CHEMICAL STRUCTURE
Nitric oxide	NO	
Nitrogen dioxide	NO_2	
Ammonia	NH_3	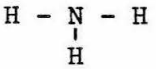
Nitrogen trioxide	NO_3	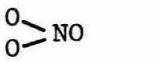
Dinitrogen pentoxide	N_2O_5	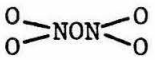
Nitric acid	$HNO_3(HONO_2)$	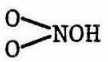
Nitrous acid	$HNO_2(HONO)$	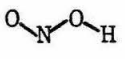
Peroxyacetylnitrate	PAN	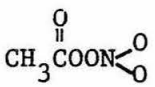
Methyl nitrite	$MeNO_2$ (RONO)	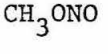
Methyl nitrate	$MeNO_3(RONO_2)$	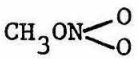
Peroxynitric acid	HO_2NO_2(PNA)	
Peroxyalkylnitrates	RO_2NO_2(PALN)	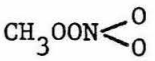
Ammonium nitrate	NH_4NO_3	

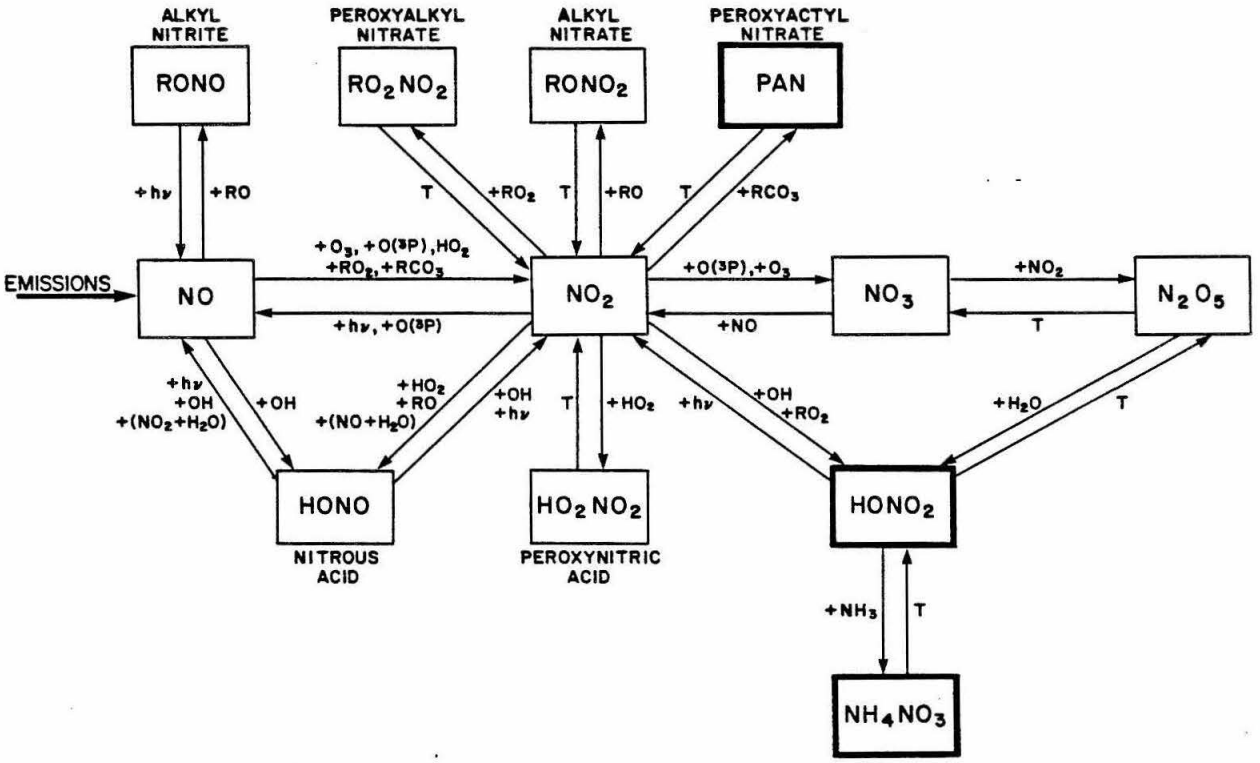

FIGURE 7

Schematic Representation of the Gas Phase Nitrogen Oxides Chemistry Including Reaction Paths for Nitrate Formation

Other than direct emission the specific reaction pathways that produce nitric acid are

$$NO_2 + OH \xrightarrow{18} HONO_2 \qquad (26)$$

$$NO_2 + RO_2 \xrightarrow{40} HONO_2 + RCO_3 \qquad (27)$$

$$N_2O_5 + H_2O \xrightarrow{46} 2HONO_2 \qquad (28)$$

During the day, reaction 18 is the dominant route for producing gas phase $HONO_2$.[61-63] At night homogeneous hydrolysis of dinitrogen pentoxide (N_2O_5) by reaction 46 can become important. Some controversy exists about the magnitude of this rate constant. In the following calculations an upper limit, due to Morris and Niki,[64] has been used. Because of the uncertainty associated with the kinetics of this mechanism step a subsequent section presents a more detailed analysis of the effects of reducing k_{46}. Further information about individual reaction steps or the photochemistry of the polluted troposphere can be found in the review articles [54-63].

An estimate of the likely ambient concentration levels of the nitrogen-containing species shown in Table 5 can be found by simulating the conditions occuring in smog chambers. A typical calculation is reported in Table 6, for an experiment carried out at the Statewide Air Pollution Research Center of the University of California, Riverside. The results indicate that at the end of the experiment most of the nitrogen was in the form of NO_2, nitric acid and PAN. For this particular example the predicted levels of O_3, NO and NO_2 agreed quite well with the concentrations observed in the smog chamber[11,12]. An indication of the lifetimes for each species can also be been inferred from

TABLE 6

Predicted Concentration of Nitrogen Containing Species for Smog Chamber Experiment SUR-119J

SPECIES	CONCENTRATION (ppm)					
	0(min)	60(min)	120(min)	180(min)	240(min)	300(min)
NO_2	$4.1x10^{-2}$	$1.6x10^{-1}$	$2.3x10^{-1}$	$2.5x10^{-1}$	$2.5x10^{-1}$	$2.3x10^{-1}$
HNO_4	0	$2.2x10^{-5}$	$4.6x10^{-5}$	$8.4x10^{-5}$	$1.3x10^{-4}$	$1.8x10^{-4}$
NO	$3.01x10^{-1}$	$1.7x10^{-1}$	$8.7x10^{-2}$	$4.4x10^{-2}$	$2.6x10^{-2}$	$1.6x10^{-2}$
HNO_2	$1.2x10^{-2}$	$6.9x10^{-3}$	$2.8x10^{-3}$	$1.1x10^{-3}$	$5.4x10^{-4}$	$3.3x10^{-4}$
PAN	0	$8.8x10^{-4}$	$3.1x10^{-3}$	$6.2x10^{-3}$	$1.0x10^{-2}$	$1.4x10^{-2}$
RONO	0	$1.0x10^{-3}$	$8.0x10^{-4}$	$4.6x10^{-4}$	$2.5x10^{-4}$	$1.3x10^{-4}$
NO_3	0	$2.3x10^{-8}$	$1.7x10^{-7}$	$7.8x10^{-7}$	$2.2x10^{-6}$	$4.6x10^{-6}$
RNO_4	0	$6.6x10^{-4}$	$1.4x10^{-3}$	$2.4x10^{-3}$	$3.6x10^{-3}$	$4.9x10^{-3}$
$2N_2O_5$	0	$2.3x10^{-6}$	$2.4x10^{-5}$	$1.2x10^{-4}$	$3.4x10^{-4}$	$6.6x10^{-4}$
RNO_3	0	$2.4x10^{-4}$	$5.7x10^{-4}$	$8.9x10^{-4}$	$1.2x10^{-3}$	$1.4x10^{-3}$
HNO_3	0	$1.2x10^{-2}$	$2.8x10^{-2}$	$4.5x10^{-2}$	$6.2x10^{-2}$	$8.0x10^{-2}$
NT [Nitrogen Balance]	0.3540	0.3539	0.3539	0.3539	0.3539	0.3539

(a) Initial conditions for smog chamber experiment SUR119J: [NO] = 0.301, [NO_2] = 0.041, [HNO_2] = 0.012, [CO] = 7.45, [HCHO] = 0.038, [RCHO] = 0.023, [ALK] = 0.358, [OLE] = 0.039, [C_2H_4] = 0.043, [ARO] = 0.07, [H_2O] = 15500.0, [O_2] = 210000.0, [M] = 1000000.0, Total Nitrogen (ppmV) = 0.354, RHC (ppmV) = 0.548, NO_x/RHC (ppmv/ppmV) = 0.642, Relative Humidity (%) = 58.5-53.0, Temperature (°C) = 30.5-33.1, Photolysis rate (min^{-1}) = 0.32, O_3 wall loss rate (min^{-1}) = 2.3×10^{-3}, Chamber dilution (min^{-1}) = 2.9×10^{-4}.

these experiments. The characteristic eigenvalue spectrum and associated reaction times are shown in Figure 8. Of the species shown in Figure 7, only PAN, the higher peroxyacylnitrates analogues, or nitric acid can be expected to be major sinks for NO_x. In passing it is useful to note that as the ambient temperature increases the role of PAN as a NO_2 sink rapidly decreases.

One feature of the mechanism that simplifies study of the interconversion between species is the fact that atomic nitrogen is conserved. The conservation constraint for nitrogen (NT) is given by

$$NT = [NO] + [NO_2] + [NO_3] + [HONO] + [HONO_2] + [HO_2NO_2] + [RONO] + [RONO_2] + [RO_2NO_2] + 2[N_2O_5] + [PAN] \quad (29)$$

This constraint, in combination with the transport and chemical processes described by (1), provides an ideal way to trace the flow of nitrogen oxides from their emission until their ultimate removal from the airshed. The next section of this paper describes a scheme for adding ammonium nitrate and ammonia to the nitrogen mass balance.

XII. FORMATION OF AMMONIUM NITRATE AEROSOL

In an urban atmosphere nitrogen oxides emissions can undergo photochemical oxidations that result in the formation of organic as well nitric acids. If ammonia (NH_3) is present, some of these compounds can be neutralized.[65-67] The mass balance on nitrogen can be completed by incorporating a calculation scheme that describes the formation of ammonium nitrate (NH_4NO_3) aerosol. Based on the work of Stelson and Seinfeld[68,69], the approach uses fundamental thermodynamic principles to find the equilibrium dissociation constant, K, for the ammonia,

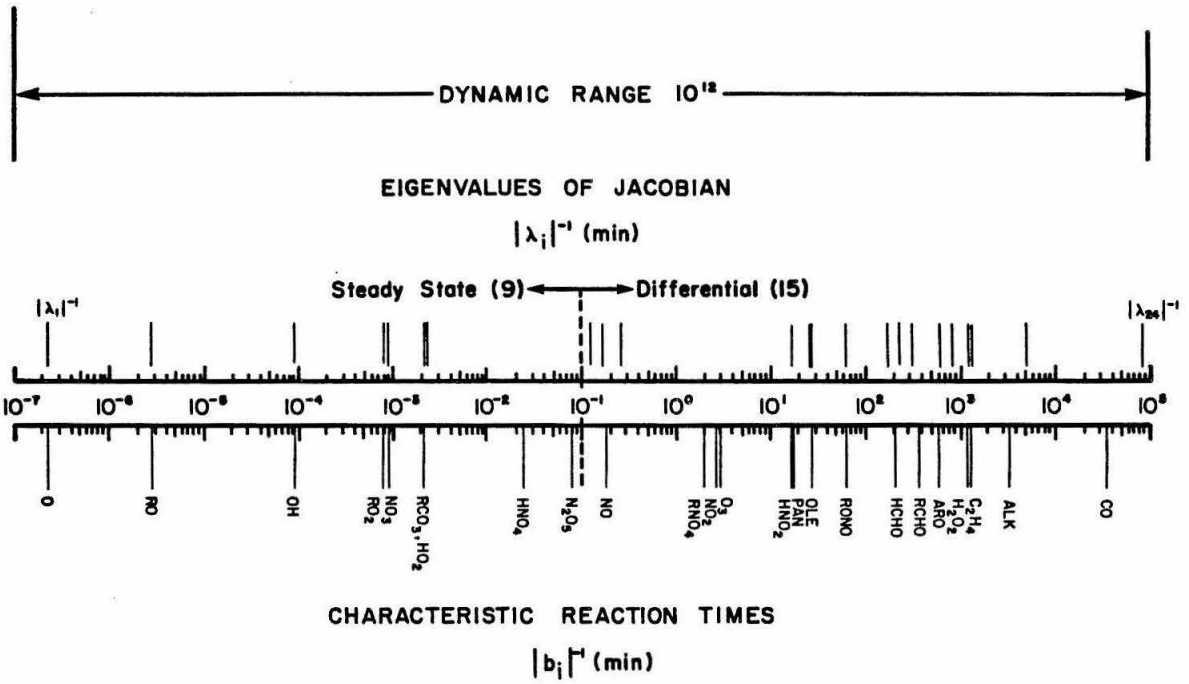

FIGURE 8

Typical Eigenvalue Spectrum and Characteristic
Reaction Times for the Photochemical Mechanism of McRae et al. (5)

nitric acid and ammonium nitrate system

$$NH_4NO_3(\text{aerosol}) \overset{K}{\longleftrightarrow} NH_3(g) + HONO_2(g) \qquad (30)$$

This system is shown schematically in Figure 9. Given the dissociation constant K,

$$K = [NH_3(g)][HONO_2(g)] \qquad (31)$$

it is a straightforward task to determine the equilibrium concentration of ammonium nitrate given the concentrations of ammonia and nitric acid, respectively. Evidence for the existence of an ammonium nitrate equilibrium in the atmosphere has been found by making simultaneous measurements of ammonia and nitric acid and comparing the data against calculated dissociation constants.[70,71]

In the study by Stelson and Seinfeld,[68,69] it was found that both the dissociation constant and the physical state of ammonium nitrate was a function of temperature and relative humidity. Ammonium nitrate is found as a solid if the relative humidity is less than that of deliquescence (RHD) given by

$$\ln RHD = 723.7/T + 1.7037 \qquad (32)$$

where T is in ^{o}K. Above the relative humidity of deliquescence ammonium nitrate exists in the aqueous phase. No ammonium nitrate should be present if the product of the concentrations of ammonia and nitric acid is smaller than the dissociation constant. Dissociation constants for typical atmospheric conditions range from 0.04 $(ppb)^2$ at $5^{o}C$ and 90% RH to 1400 $(ppb)^2$ at $40^{o}C$ and a RH of 30%. The particular details of the calculation procedure are described in Russell et al.[13]

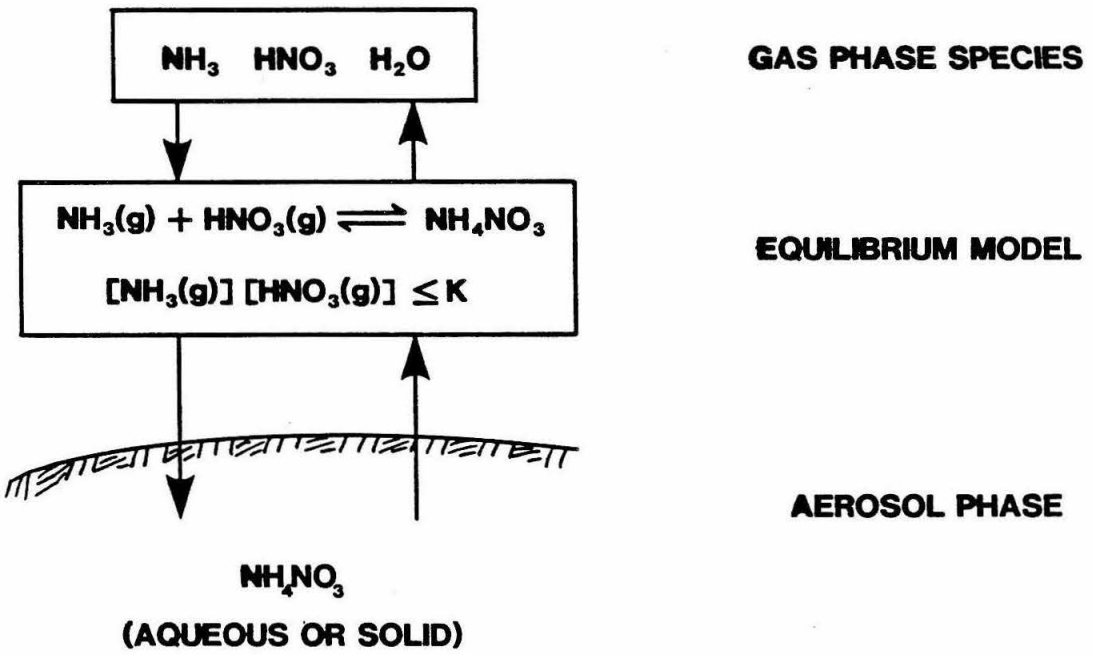

FIGURE 9

Schematic Representation of the Equilibrium Model for Ammonium Nitrate (NH_4NO_3) Formation

and will not be repeated here. Ammonium nitrate aerosol deposition is treated in the same manner as gaseous deposition. A value for the approximate deposition velocity was estimated from the experimental measurements of the deposition rates of NH_4^+ and NO_3^-.[25]

XIII. EVALUATION OF THE MODEL PERFORMANCE

Once the model has been formulated the next step is to evaluate its ability to predict ambient concentrations of both the gas phase and particulate species. The data required for such tests include; pollutant emissions, observed air quality and the prevailing meteorology. The particular day chosen for this study was 27 June 1974, a period typical of the severe smog episodes that are experienced in Southern California. These days are characterized by high oxidant and nitric acid levels. For this study, the air parcel trajectory was selected so that it crossed the airshed. The trajectory started near the ocean at midnight, then proceeded east over Los Angeles, and finally passed over Upland at 1600 Pacific Standard Time (PST). By initiating the calculations over the ocean the influence of initial conditions on the pollutant loadings in the air column is very small.

One of the most important inputs is a comprehensive detailed and accurate emission inventory, constructed at a level of detail consistent with the required spatial, temporal and chemical resolution of the model. In this study emissions from 130 different source categories were distributed over the region shown in Figure 1. A summary of the daily totals and the distribution between mobile and stationary source classes is shown in Table 7. Diurnal variations in emission rates were resolved to within one hour in order that the model

TABLE 7

Summary of Estimated 1974 Daily South Coast Air Basin Emissions

SPECIES	TOTAL EMISSIONS (kg/day)	SOURCE CLASS CONTRIBUTION (%) MOBILE	STATIONARY
Carbon monoxide (CO)	8,610,000	98.8	1.2
Nitrogen oxides (NO_x)	1,320,000	62.3	37.7
Sulfur oxides (SO_x)	427,000	13.7	86.3
Total Hydrocarbons (THC)	3,379,000	30.0	70.0
Reactive Hydrocarbons (RHC)	1,290,000	71.0	29.0
Ammonia (NH_3)	150,000	3.0	97.0

predictions would be compatible with the averaging time used in making ambient air quality measurements. The overall spatial distribution of NH_3, nitrogen oxides, reactive hydrocarbons and carbon monoxide emissions in the South Coast Air Basin is shown in Figure 10. The largest spike in the NH_3 diagram is centered over the town of Chino on the prevailing upwind side of the city of Riverside, and results from the intensity of livestock operations in that area. Further descriptions of the emission inventories for nitrogen oxides, hydrocarbons and ammonia for June 26 through 28, 1974, are available.[6,13]

Both the gas phase and aerosol pollutant concentration predictions have been compared against observations reported at monitoring close to the trajectory path. In evaluating the model performance, the predictions were compared against measurements of O_3, NO_2, NO, NH_4NO_3, NO_3^- and NH_4^+.[6,13] In both studies agreement between the measured and calculated concentrations was good. Some of the results are shown in Figure 11a and b. The ability of a model to describe ambient concentrations of gases is only one indication of the validity of the treatment for surface deposition. Extensive experiments in the air basin are required for definitive evaluation of the performance of the deposition calculations. At present, the needed experimental data do not exist.

XVI. CALCULATION OF ACIDIC DEPOSITION FLUXES

The basic objective of this study is to present a methodology that can be used to determine the magnitude of acid deposition resulting from the oxidation of nitrogen oxides emissions. In the subsequent calculations acid deposition is defined as the surface flux of species with immediately available protons minus proton scavenging species.

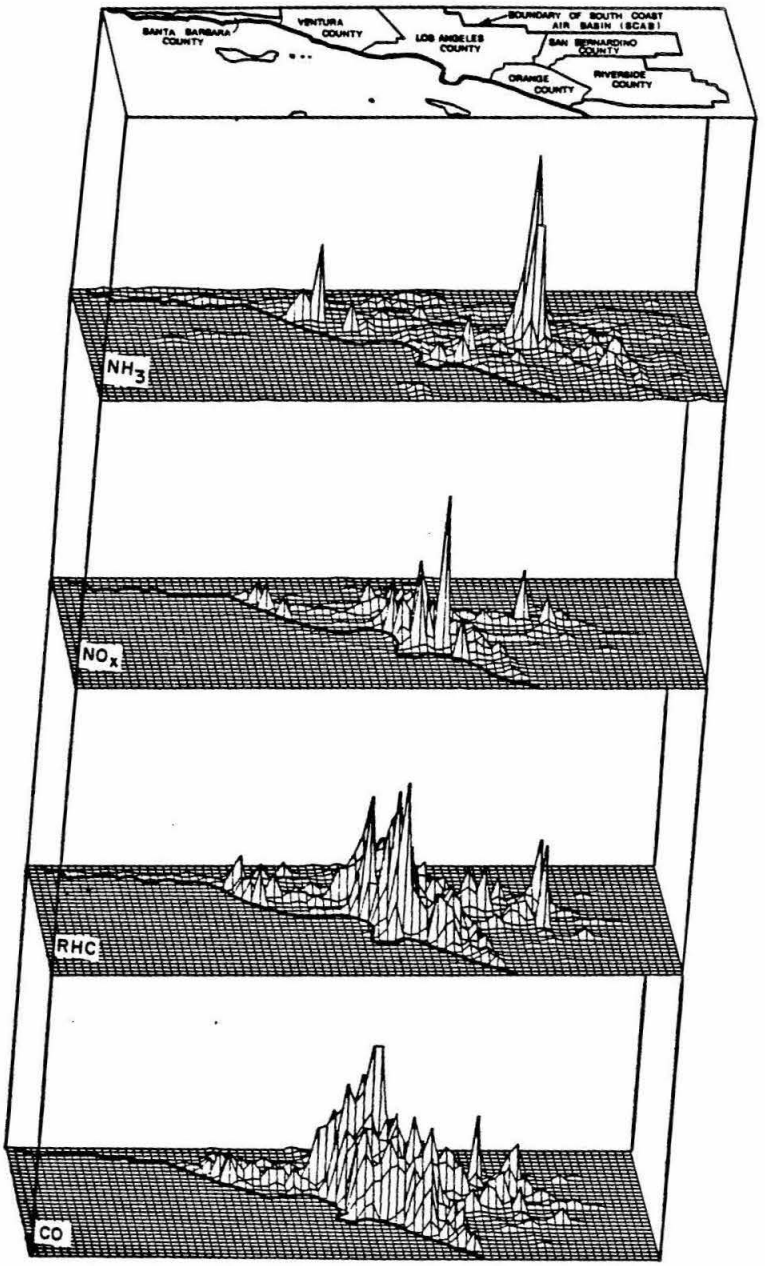

FIGURE 10

Spatial Variation of the Daily Average Emissions of Ammonia (NH_3), Nitrogen Oxides (NO_x), Reactive Hydrocarbons (RHC) and Carbon Monoxide (C)) Over the South Coast Air Basin for the Period June 1974

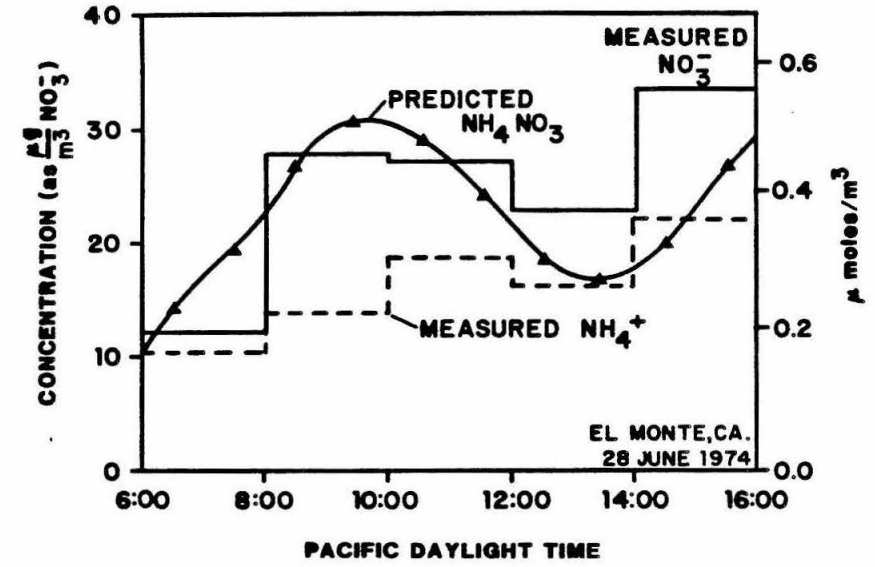

(a)

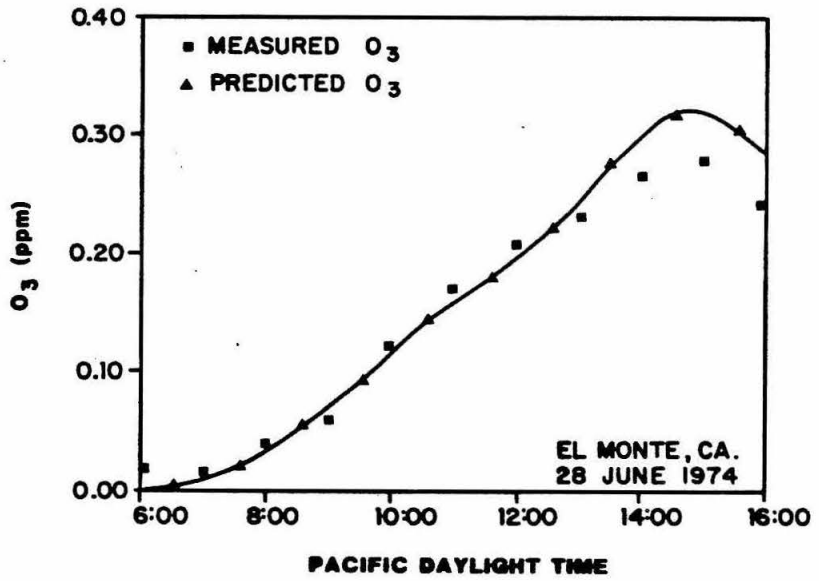

(b)

FIGURE 11

Comparison of Model Predictions Against Ambient Data for (a) NH_4NO_3 and (b) Ozone on 28 June 1974 at El Monte, California

Thus, considering just the NH_3-HNO_3-NH_4NO_3-HONO system, the net acid deposition is given by

$$\{\text{Acid Flux}\} = \{HNO_3 \text{ Flux}\} + \{\text{HONO Flux}\} - \{NH_3 \text{ Flux}\} \qquad (33)$$

This definition, while adequate for many circumstances, may require modification to account for reactions in the receiving ecosystem, such as $NH_4^+ + 2O_2 \longrightarrow 2H^+ + NO_3^- + H_2O$ as well as the slightly acidic character of NH_4NO_3. The deposition of sulfate or the possible acid producing reactions involving deposited NO_2 and SO_2 have not been included in the present study.

By using the model (1) a mass balance on nitrogen-containing species can be constructed to account for emissions and reaction products, as well as total surface deposition. The instantaneous deposition flux of total nitrogen, shown in Figure 12, demonstrates the pronounced influence of atmospheric stability. The deposition flux is greatest in the afternoon because of rapid mixing. By comparison, the net flux at night is much lower even though there is more nitrogen-containing material in the air column. The importance of this result is further highlighted in Figure 13 which depicts the balance between deposited nitrogen oxides emissions and those emissions remaining in the air column. Approximately 35% (by mole equivalent) of the nitrogen oxides emissions are deposited during the day. Of the 65% of the nitrogen-containing pollutants that remain in the air parcel, 41% is nitric acid at the end of the trajectory studied. The remaining nitric acid could be expected to deposit out on subsequent days.

Deposition of both acidic and basic species occurs along the whole trajectory as shown in Figure 14. In this figure, the fraction

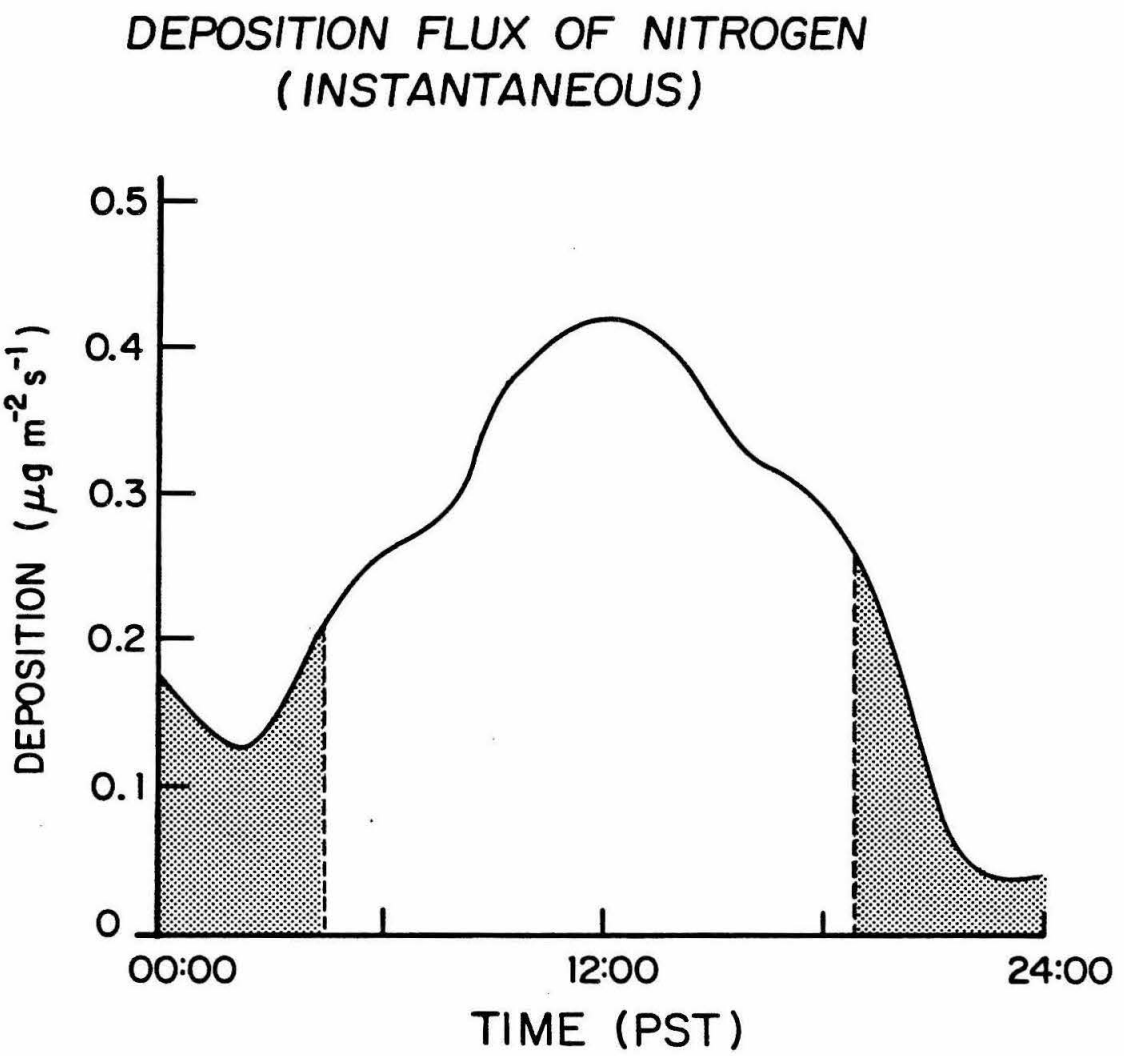

FIGURE 12

Diurnal Variation in the Instantaneous Deposition Flux of Nitrogen

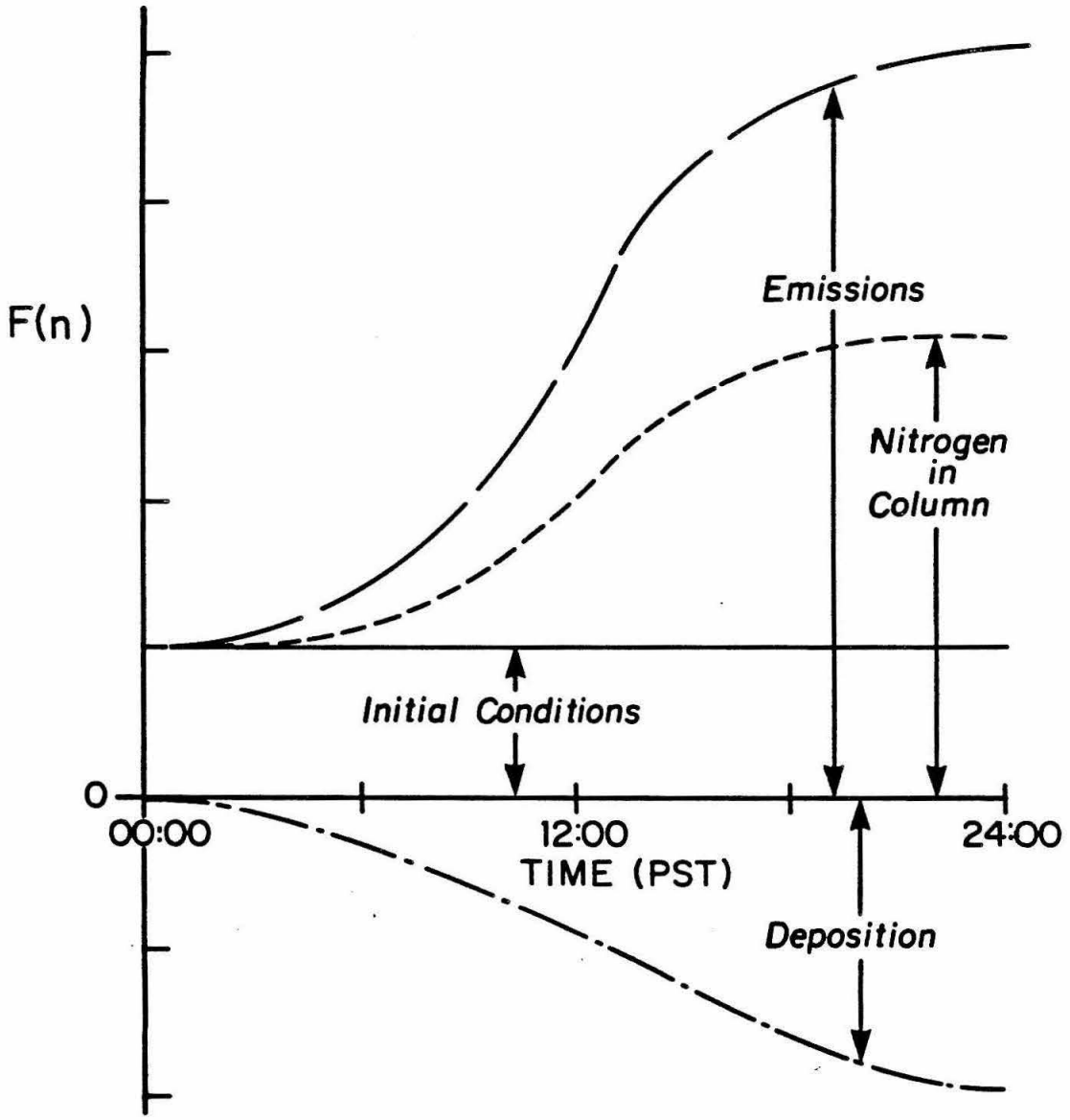

FIGURE 13

Cumulative Nitrogen Balance Illustrating
the Fractional [f(n)] Contribution from:
Initial Conditions, Direct Emissions into the Air Column and
the Removal by Dry Deposition

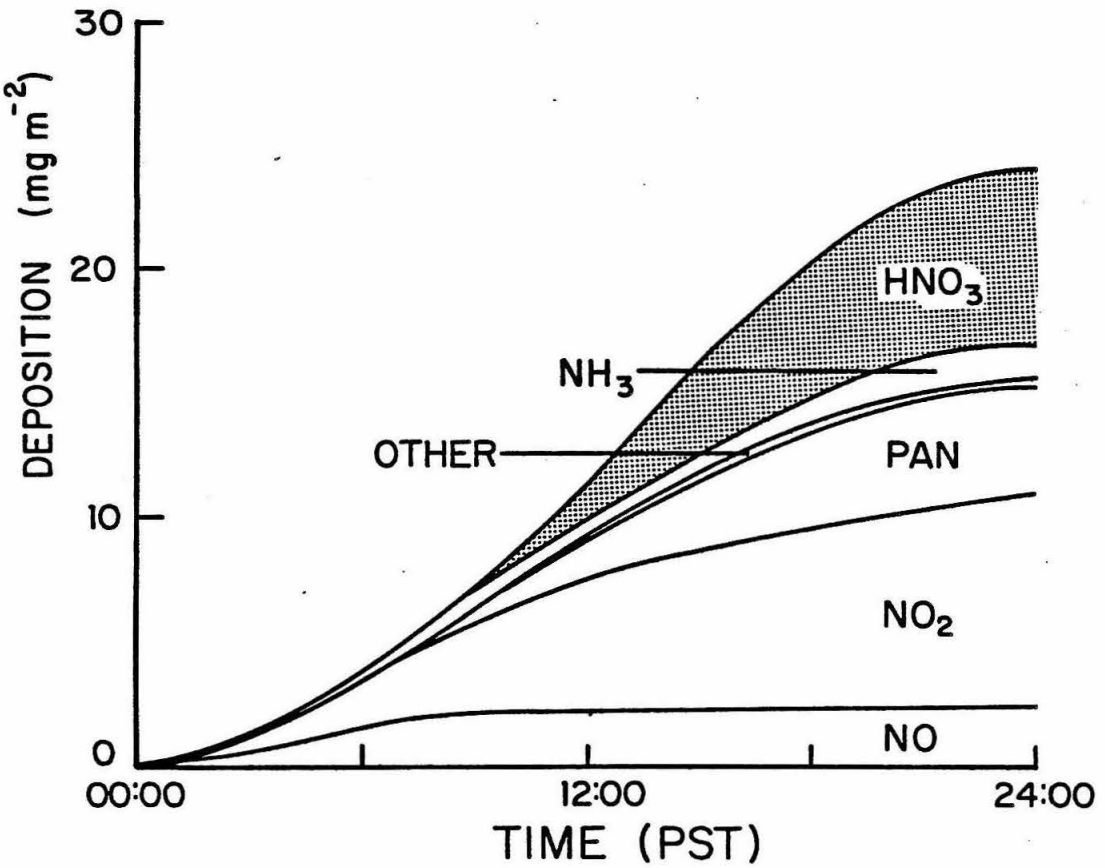

FIGURE 14

Cumulative Deposition of Nitrogen Containing Species

labelled as 'other' consists primarily of ammonium nitrate. In the early morning near the coast, the deposition rate of ammonia is higher than that of the nitrogenous acids. The reason for this is that the nitrogen oxides emissions have not reacted to form nitric acid. After sunrise the deposition rate increases, and nitric oxides start to oxidize to form nitric acid. This leads to a net acid flux. This trend continues until sunset when the atmosphere becomes more stable, decreasing the deposition rate. The nitric acid burden in the air parcel is still much greater than ammonia. Of the nitrogen containing material that is deposited during the first day the dominant fractions are: nitric acid (30%), peroxyacetyl nitrate (20%), nitrogen dioxide (40%) and ammonia (6%). Table 8 summarizes the net acid and nitrogen deposition at the end of the trajectory.

The predicted net dry acid deposition, from Table 8, of 422 micro eq m^{-2} can be compared to the findings of Liljestrand and Morgan[4] for wet deposition. Liljestrand and Morgan estimated the wet flux of nitrogenous acids to be 0.016 eq m^{-2} per year. By comparison, the results of this study would suggest that the dry deposition flux of acidic materials would be of the order of 0.19 eq m^{-2} per year. Dry deposition appears to account for a much greater flux of acid than wet deposition. It should be kept in mind that the estimate obtained in this study should be an upper limit due to the deposition model used and trajectory chosen.

XV. DYNAMICS OF NITRIC ACID PRODUCTION

As shown in the previous section nitric acid was the dominant fraction of the deposited acidic materials. The diurnal variation of the contributions to its production, from the different reaction

TABLE 8

Integrated Fluxes of Nitrogen Containing Species and Associated Acid Deposition for 24-hr Period Along a Representative Trajectory[a]

SPECIES	DEPOSITED NITROGEN $\mu g\ m^{-2}$	ACID DEPOSITION $\mu eq\ m^{-2}$	AMMONIA RELATED NITROGEN DEPOSITION $\mu g\ m^{-2}$
NO	2422(10.4)		
NO_2	8742(37.7)		
PAN	4477(19.3)		
$HONO_2$	7255(31.3)	518	
HONO	26.4(0.1)	1.9	
NH_4NO_3	277(1.2)		277(16.7)
NH_3	---	-98[b]	1377(83.3)
TOTAL	23199(100%)	422	1654(100%)

[a] 27 June 1974 Upland trajectory

[b] Negative flux corresponds to neutralization of $HONO_2$ by NH_3

[c] Total nitrogen deposition (excluding NH_3)

pathways, is shown in Figure 15. As expected, the NO_2-OH reaction dominates during the day. Immediately after sunset, however, most of the nitric acid is predicted to be formed by the homogeneous hydrolysis of N_2O_5. The rate constant used for that reaction, $k_{46} = 1.5 \times 10^{-6}$ ppm^{-1} $-min^{-1}$, is, as mentioned previously, believed to be an upper limit. Because some controversy exists about the magnitude of k_{46}, it was decided to test the sensitivity of nitric acid formation to k_{46}. This can be done by investigating the reactions involving N_2O_5 below.

$$NO_2 + O \xrightarrow{6} NO_3 \qquad k_6 - 3600 \quad ppm^{-1}\ min^{-1} \qquad (34)$$

$$NO_2 + O_3 \xrightarrow{7} NO_3 \qquad k_7 - 0.05 \quad ppm^{-1}\ min^{-1} \qquad (35)$$

$$NO + NO_3 \xrightarrow{8} NO_2 \qquad k_8 - 27200 \quad ppm^{-1}\ min^{-1} \qquad (36)$$

$$NO_2 + NO_3 \xrightarrow{44} N_2O_5 \qquad k_{44} - 3900 \quad ppm^{-1}\ min^{-1} \qquad (37)$$

$$N_2O_5 \xrightarrow{45} NO_2 + NO_3 \qquad k_{45} - 6.9 \quad ppm^{-1}\ min^{-1} \qquad (38)$$

$$N_2O_5 + H_2O \xrightarrow{46} 2HNO_3 \qquad k_{46} - 3x10^{-6} \quad ppm^{-1}\ min^{-1} \qquad (39)$$

Homogeneous hydrolysis of N_2O_5, is not well understood. The rate constant given (k_{46}) is an upper bound by Morris and Niki,[64] with the actual rate constant possibly being considerably less. The reason for this is that measurement of the rate constant is plagued by the rapid heterogeneous reaction of N_2O_5 with the surfaces of the reaction chamber. Nevertheless the dynamics of the N_2O_5-NO_3-HNO_3 system can still be studied. The rate expression for NO_3 and N_2O_5, using the above system, are

$$\frac{d[NO_3]}{dt} = k_6[NO_2][O]+k_7[NO_2][O_3]-k_8[NO_3][NO]-k_{44}[NO_2][NO_3]+k_{45}[N_2O_5] \qquad (40)$$

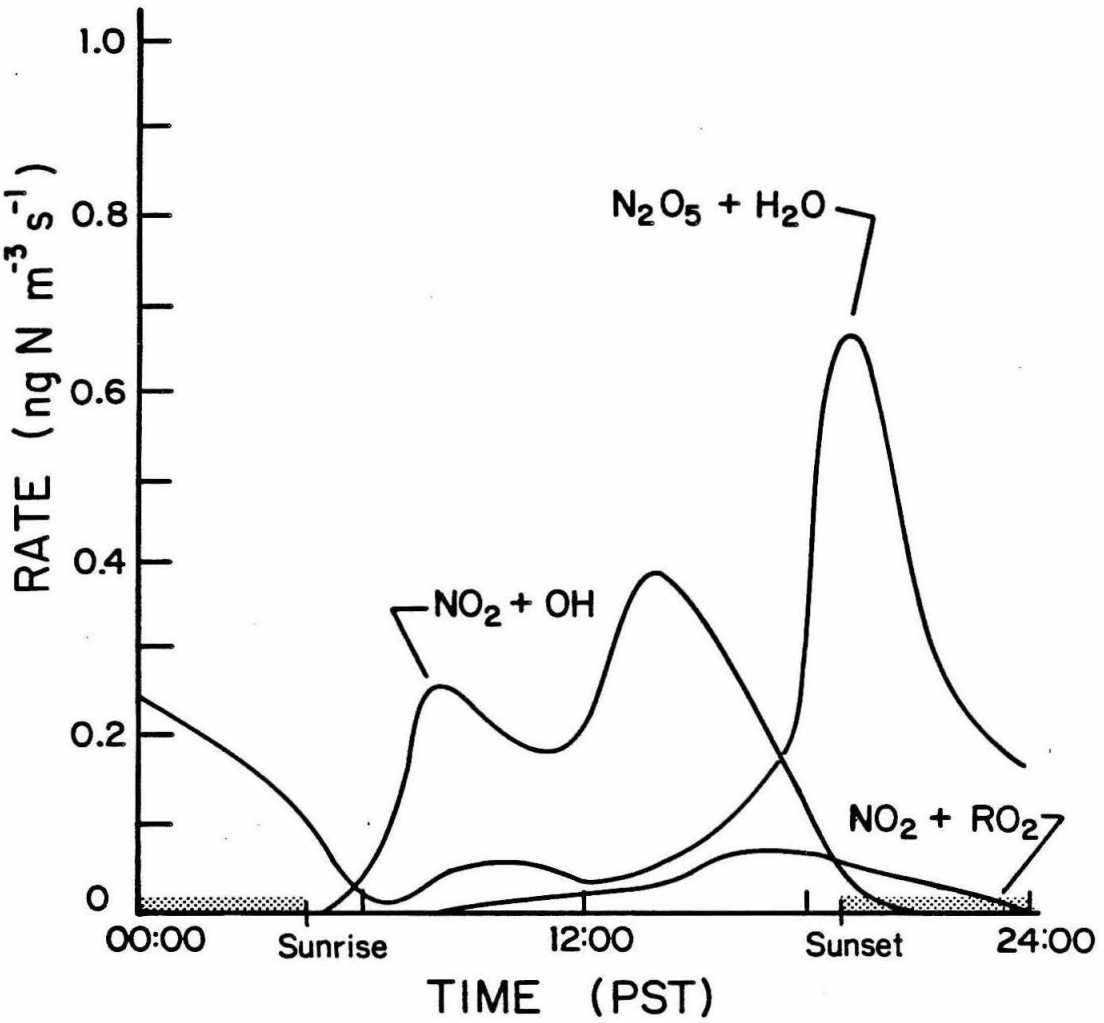

FIGURE 15

Diurnal Variation in the Contribution of Three Different Reaction Pathways to the Formation of Gas Phase Nitric Acid ($HONO_2$)

and

$$\frac{d[N_2O_5]}{dt} = k_{44}[NO_2][NO_3]-k_{45}[N_2O_5]-k_{46}[N_2O_5][H_2O] \tag{41}$$

Both these species have very short lives, and steady state approximations can be made. Simultaneously solving for NO_3 and N_2O_5 concentrations as a function of other concentrations gives

$$[NO_3] = \frac{\{k_6[O][NO_2]+k_7[O_3][NO_2]\}\{k_{45}+k_{46}[H_2O]\}}{k_8k_{46}[NO][H_2O]+k_{45}k_8[NO]+k_{44}k_{46}[NO_2][H_2O]} \tag{42}$$

and

$$[N_2O_5] = \frac{k_{44}[NO_2]\{k_6[O][NO_2]+k_7[O_3][NO_2]\}}{k_8k_{46}[NO][H_2O]+k_{45}k_8[NO]+k_{44}k_{46}[NO_2][H_2O]} \tag{43}$$

Figure 15 indicated that the homogeneous N_2O_5 hydrolysis is important only during the nighttime when O atom concentrations are negligible. Also the NO concentrations are very low at night, on this occasion, except near the ground. With this in mind, the expressions can be simplified to give the rate of nitric acid formation by hydrolysis as

$$\frac{d[HNO_3]}{dt} = \frac{2\ k_{46}k_{47}k_7[H_2O][O_3][NO_2]^2}{k_{46}k_{44}[NO_2][H_2O] + k_{45}k_8[NO]} \tag{44}$$

Using typical nighttime, ground level concentrations for the various species shown in Table 5, the production of nitric can be approximated as

$$\frac{d[HNO_3]}{dt} = \frac{2\ k_{46}k_{47}k_7[H_2O][O_3][NO_2]^2}{k_8k_{45}[NO]} \tag{45}$$

If the NO concentration is much lower, as it is above the inversion, the first term dominates, and (44) simplifies to

$$\frac{d[HNO_3]}{dt} = 2\, k_7[O_3][NO_2] \qquad (46)$$

and the rate of HNO_3 formation can be seen to be much greater than at ground level. This expression is insensitive to uncertainty in k_{46}, and is approximately valid as long as

$$k_{45}k_8[NO] << k_{46}k_{44}[NO_2][H_2O] \qquad (47)$$

The surprising result from this analysis is that aloft the production of HNO_3 by N_2O_5 hydrolysis is insensitive to k_{46}. Bcause most of the N_2O_5 hydrolysis occurs aloft where [NO] is low, the column averaged total production of HNO_3 by N_2O_5 is relatively insensitive to revisions in k_{46}. A test using a hydrolysis rate constant one fifth of the upper limit gave results essentially unchanged to what was found previously, though slightly less nitric acid was produced near the ground. The results drawn from this analysis are dependent on the dynamics of NO_3. In the present calculations the effect of aerosol scavenging [73,74] have been ignored. The model predicts a rapid rise and fall in the concentration of NO_3 centered about 1900 (PST). This trend and the calculated peak value of 0.065 ppb is comparable to the results reported by Platt et al[72].

In summary the production of nitric acid by homogeneous N_2O_5 hydrolysis at night could be a major source of nitric acid in the atmosphere. The analysis indicates that immediately above the inversion, where NO concentrations are very low that the production of nitric acid

at night can be comparable with that found during the day by the NO_2-OH reaction.

XVI. CONCLUSIONS

Nitrogen oxides emissions and their photochemical oxidation products are significant sources of acidic compounds in the atmosphere. A critical element of any approach directed at minimizing the environmental impacts resulting from the deposition of these materials is a reliable means for evaluating the air quality impact of alternative control measures. The primary objective of this work has been to present such a capability in the form of a model of the processes influencing the physical and chemical dynamics of nitrogen containing species over an urban area. In particular, the mathematical formulation incorporates the effects of emissions, transport, chemical conversions and surface deposition. The surface removal component of this model has several important features including, explicit treatments of the effects of surface conditions and diurnal changes in atmospheric stability. A formal procedure for determining equivalent cell average deposition velocities, needed in the numerical calculations, is also presented.

Applications of the model are illustrated by examining the fate of nitrogen oxides emitted into an urban environment. A mass balance on nitrogen containing species is constructed along a wind trajectory that traverses the South Coast Air Basin of southern California. For the particular trajectory chosen several conclusions can be drawn. Perhaps the most significant is that during one day approximately 35% of the nitrogen emitted into the air is removed by dry deposition. This short lifetime indicates that almost all of the nitrogen oxides and their acidic oxidation products could be removed within a few days travel

time from the source of the emissions. Of the nitrogen containing material that is deposited during the first day the dominant fractions are: nitric acid (30%), peroxyacetyl nitrate (20%), nitrogen dioxide (40%) and ammonia (6%). Ammonia acts to neutralize some of the deposited acids by forming ammonium nitrate. Nitric acid and peroxyacetyl nitrate are the two most abundant photochemical oxidation products remaining in the column of air. These compounds can be removed on the second and subsequent days. While there is a clear need for additional laboratory studies and field measurements these initial results provide a demonstration of how a mass balance formulation can be used to study the impact of nitrogen oxides emissions on acid deposition.

Acknowledgements This work was supported, in part, by a grant from the Andrew W. Mellon Foundation to the Environmental Quality Laboratory. Development of the photochemical model and the associated mechanism for predicting the formation of ammonium nitrate was carried out under Contracts A5-046-87, A7-169-30 and A7-187-30 from the California Air Resources Board.

References

1. Cowling, E.B. "Acid Precipitation in Historical Perspective," Environmental Science and Technology 16:110A-123A (1982).

2. Cogbill, C.V. and G.E. Likens "Acid Precipitation in the Northeastern United States," Water Resources Research 10(6):1133-1137 (1974).

3. National Acid Precipitation Assessment Plan (The Inter Agency Task Force on Acid Precipitation, Council on Environmental Quality, Washington, D.C., 1981)

4. Morgan, J.J. and H.M. Liljestrand "Spatial Variation of Acid Precipitation in Southern California," Environmental Science and Technology 15:333-339 (1980).

5. McRae, G.J., W.R. Goodin and J.H. Seinfeld "Development of a Second Generation Mathematical Model for Urban Air Pollution: I Model Formulation," Atmospheric Environment 16:679-696 (1982).

6. McRae, G.J. and J.H. Seinfeld "Development of a Second-Generation Mathematical Model for Urban Pollution II: Model Performance Evaluation," Atmospheric Environment (in press, 1982).

7. Seinfeld, J.H. Air Pollution: Physical and Chemical Fundamentals New York:McGraw-Hill Book Company (1975).

8. Goodin, W.R., G.J. McRae and J.H. Seinfeld "A Comparison of Interpolation Methods for Sparse Data: Application to Wind and Concentration Fields," J. Applied Meteorology 18:761-771 (1979).

9. Goodin, W.R., G.J. McRae and J.H. Seinfeld "Reply to Comments," J. Applied Meteorology 20:92-94 (1981).

10. Goodin, W.R., G.J. McRae and J.H. Seinfeld "An Objective Analysis Technique for Constructing Three-Dimensional, Urban Scale Wind Fields," J. Applied Meteorology 19:98-108 (1979).

11. Falls, A.H. and J.H. Seinfeld "Continued Development of a Kinetic Mechanism for Photochemical Smog," Environmental Science and Technology 12:1398-1406 (1978).

12. Falls, A.H., G.J. McRae and J.H. Seinfeld "Sensitivity and Uncertainty of Reaction Mechanisms for Photochemical Air Pollution," International J. Chemical Kinetics 11:1137-1162 (1979).

13. Russell, A.G., G.J. McRae and G.R. Cass "Mathematical Modeling of the Formation and Transport of Ammonium Nitrate Aerosol," Atmospheric Environment (in press, 1982).

14. McRae, G.J., W.R. Goodin and J.H. Seinfeld "Numerical Solution of the Atmospheric Diffusion Equation for Chemically Reacting Flows," J. Computational Physics, 45:1-42 (1982).

15. Liu M-K and J.H. Seinfeld "On the Validity of Grid and Trajectory Models of Urban Air Pollution," Atmospheric Environment 9:555-574 (1975).

16. Chamberlain, A.C. "Transport of Gases to and from Grass and Grass-Like Surfaces," Proc. Royal Society Series A 290:236-265 (1966).

17. Hill, A.C. and E.M. Chamberlain "The Removal of Water Soluble Gases from the Atmosphere by Vegetation," in Atmosphere-Surface Exchange of Particulate and Gaseous Pollutants (ERDA Publication, NTIS Number CONF-740921, 1974) pp. 153-169.

18. Kneen, T. and W. Strauss "Deposition of Dust from Turbulent Gas Streams," Atmospheric Environment 3:55-67 (1969).

19. Liu, T.Y.H. and T.A. Ilori "Aerosol Deposition in Turbulent Pipe Flow," Environmental Science and Technology 8:351-356 (1974).

20. Sehmel, G.A. and W.H. Hodgson "Predicted Dry Deposition Velocities," in Atmosphere-Surface Exchange of Particulate and Gaseous Pollutants (ERDA Publication, NTIS Number CONF-740921, 1974), pp. 399-419.

21. Slinn, W.G.N. "Dry Deposition and Resuspension of Aerosol Particles-A New Look at Some Old Problems," in Atmosphere-Surface Exchange of Particulate and Gaseous Pollutants (ERDA Publication, NTIS Number CONF-740921, 1974), pp. 1-40.

22. McMahon, T.A. and P.J. Denison "Empirical Atmospheric Deposition Parameters--A Survey," Atmospheric Environment 13:571-585 (1979).

23. Sehmel, G.A. "Particulate and Gas Dry Deposition: A Review," Atmospheric Environment, 14:983-1011 (1980).

24. Hosker, R.P. and S.E. Lindberg "Review: Atmospheric Deposition and Plant Assimilation of Gases and Particles," Atmospheric Environment 16(5):889-910 (1982).

25. Slinn, S.A. and W.G.N. Slinn "Modeling of Atmospheric Particulate Deposition to Natural Waters," in Atmospheric Pollutants in Natural Waters, ed. Steven J. Eisenriech, (Ann Arbor Science, 1982).

26. Brutsaert, W. "The Roughness Length for Water Vapor, Sensible Heat, and Other Scalars," J. Atmospheric Sciences 32:2028-2031 (1975).

27. Businger, J.A., J.C. Wyngaard, Y. Izumi and E.F. Bradley "Flux Profile Relationships in the Atmospheric Surface Layer," J. Atmospheric Science 28:181-189 (1971).

28. Dyer, A.J. and B.B. Hicks "Flux-Gradient Relationships in the Constant Flux Layer," Quarterly J. Royal Meteorological Society, 96:715-721

29. Galbally, I.E. "Ozone Profiles and Ozone Fluxes in the Atmospheric Surface Layer," Quarterly J. Royal Meteorological Society, 97:18-29 (1971).

30. Busch, N.E. "On the Mechanics of Atmospheric turbulence," in Workshop on MicroMeteorology, ed. D.A. Haugen, (American Meteorological Society, Boston, 1973).

31. Wesely, M.L. and B. Hicks "Some Factors that Affect the Deposition Rates of Sulfur Dioxide and Similar Gases on Vegetation," J. Air Pollution Control Associatio, 27:1110-1116 (1977).

32. Garland, J.A. "Dry Deposition of SO_2 and Other Gases," in Atmosphere-Surface Exchange of Particulate and Gaseous Pollutants (ERDA Publication, NTIS Number CONF-740921, 1974) pp. 212-227.

33. Garland, J.A. and S.A. Penkett "Absorption of Peroxy Acetyl Nitrate and Ozone by Natural Surfaces," Atmospheric Environment, 10: 1127-1131.

34. Wesely, M.L., B.B. Hicks, W.P. Dannevik, S. Frisella and R.B. Husar "An Eddy-Correlation Measurement of Particulate Deposition from the Atmosphere," Atmospheric Environment 11:561-563 (1977).

35. Wesely, M.L., J.A. Eastman, D.R. Cook and B.B. Hicks "Daytime Variations of Ozone Eddy Fluxes to Maize," Boundary Layer Meteorology 15:361-373 (1978).

36. Wesely, M.L.,J.A. Eastman, D.H. Stedman and E.D. Yalvac "An Eddy Correlation Measurement of NO_2 Flux to Vegetation and Comparison to O_3 Flux," Atmospheric Environment 16:815-820 (1982).

37. Owers, M.J. and A.W. Powell "Deposition Velocity of Sulfur Dioxide on Land and Water Surfaces Using a ^{35}S Tracer Method," Atmospheric Environment 8:63-68 (1974).

38. Whelpdale, D.M. and R.W. Shaw "Sulfur Dioxide Removal by Turbulent Transfer Over Grass, Snow and Water Surfaces," Tellus, 26:196-205 (1974).

39. Droppo, J.G. "Summary of Field Data on Dry Removal Rates of Gases and Particles from the Atmosphere," in Battelle Pacific Northwest Laboratory Annual Report for 1976, Part 3 Atmospheric Sciences, (Richland, Washington, 1976).

40. Slinn, W.G.N, L. Hasse, B.B. Hicks, A.W. Logan, D. Lal, P.S. Liss, K.O. Munnich, G.A. Sehmel and O. Vittori "Some Aspects of the Transfer of Atmospheric Trace Constituents Past the Air-Sea Interface," Atmospheric Environment 12:2055-2087 (1978).

41. Judekis, H.S. and A.G. Wren "Laboratory Measurements of NO and NO_2 Depositions Onto Soil and Cement Surfaces," Atmospheric Environment 12:2315-2319 (1978).

42. Anderson, V. "The Influence of Weather Upon the Amounts of Nitric and of Nitrous Acid in RainfallaAt and Near Melbourne, Australia," Quarterly Journal Royal Meteorological Society 41:99-122 (1915).

43. Hampson, R.F. and D. Garvin "Reaction Rate and Photochemical Data for Atmospheric Chemistry - 1977," (U.S. Department of Commerce National Bureau of Standards Special Publication 513, 1978).

44. Graham, R.A. and H.S. Johnston, H.S. "The Photochemistry of NO_3 and the Kinetics of the N_2O_5-O_3 System," J. Physical Chemistry, 82:254-268 (1978).

45. Graham, R.A., A.M. Winer and J.N. Pitts "Temperature Dependence of the Unimolecular Decomposition of Pernitric Acid and its Atmospheric Implication," Chemical Physics Letters 51:215-220 (1977).

46. Cox, R.A. and M.J. Roffey "Thermal Decomposition of Peroxyacetylnitrate in the Presence of Nitric Oxide," Environmental Science and Technology 11:900-906 (1977).

47. Baldwin, A.C., J.R. Barker, D.M. Golen and D.G. Hendry "Photochemical Smog Rate Parameter Estimates and Computer Simulation," J. Physical Chemistry 81:2483-2492 (1977).

48. Batt, L. and G.N. Rattray "The Reaction of Methoxy Radicals with Nitric Oxide and Nitrogen Dioxide," International J. of Chemical Kinetics 11:1183-1196.

49. Baker, G. and R. Shaw "Reactions of Methoxyl, Ethyoxyl, and t-Butoxyl with Nitric Oxide and Nitrogen Dioxide," J. Chemical Society (London), 5:6965-6970 (1965).

50. Simonaitis, R. and J.I. Heicklen "Reactions of HO_2 with NO and NO_2," J. Physical Chemistry, 78:653-657 (1974)

51. Chemical Kinetics and Photochemical Data for Use in Stratospheric Modeling -- Evaluation Number 4, (Jet Propulsion Laboratory Report Number 81-3, Jet Propulsion Laboratory, Pasadena, California, 1981).

52. Sander, S.P. and R.T. Watson "Kinetics Studies of the Reactions of CH_3O_2 with NO, NO_2, and CH_3O_2 at 298K," J. Physical Chemistry 84:1664-1674 (1980).

53. Baulch, D.L., R.A. Cox, R.f. Hampson, J.A. Kerr, J. Troe and R.T. Watson "Evaluated Kinetic and Photochemical Data for Atmospheric Chemistry," J. Physical Chemistry Reference Data 9:295 (1980).

54. Demerjian, J., J.A. Kerr, and J.G. Calvert "The Mechanism of Photochemical Smog Formation," Advances in Environmental Science and Technology, 4, (1974).

58. Heiklen, J. Atmospheric Chemistry New York:Academic Press (1976).

59. Cox, R.A. "Tropospheric Chemistry of Nitrogen Oxides - A Summary of the Status of Chemical Kinetic Data," National Bureau of Standards Special Publication No. 557 (Washington, D.C.: U.S. Government Printing Office, 1979).

60. Seinfeld, J.H. "Lectures in Atmospheric Chemistry," AIChE Monograph Series 76(12):98 pp (1980).

61. Calvert, J.G. and W.R. Stockwell "The Mechanism and Rates of the Gas Phase Oxidations of Sulfur Dioxide and the Nitrogen Oxides in the Atmosphere," in Acid Precipitation: SO_2, NO, and NO_2 Oxidation Mechanisms: Atmospheric Considerations (Ann Arbor Science Publishers Inc., 1982).

62. Spicer, C.W. "The Fate of Nitrogen Oxides in the Atmosphere," Advances in Environmental Science and Technology 7:163-261 (1974).

63. Nitrogen Oxides (National Academy of Sciences, Washington, D.C., 1977).

64. Morris, E.D. and H. Niki "Reaction of Dinitrogen Pentoxide with Water," J. Physical Chemistry 77:1929-1932 (1973).

65. Orel, A.E. and J.H. Seinfeld "Nitrate Formation in Atmospheric Aerosols," Environmental Science Technology 11:1000 (1977).

66. Nitrates: An Environmental Assessment (National Academy of Sciences, Washington, D.C., 1978).

67. Barnes, H.M. Ed. "Formation and Fate of Atmospheric Nitrates," U.S. Environmental Protection Agency Report No. EPA-600/9-81-025 (1981).

68. Stelson, A.W. and J.H. Seinfeld "Relative Humidity and Temperature Dependence of the Ammonium Nitrate Dissociation Constant," Atmospheric Environment 16:983-992 (1982).

69. Stelson, A.W. and J.H. Seinfeld "Relative Humidity and pH Dependence of the Vapor Pressure of Ammonium Nitrate-Nitric Acid Solutions at 25°C," Atmospheric Environment 16:993-1000 (1982).

70. Stelson, A.W., S.K. Friedlander and J.H. Seinfeld "A Note on the Equilibrium Relationship Between Ammonia and Nitric Acid and Particulate Ammonium Nitrate," Atmospheric Environment 13:369-371 (1979).

71. Doyle, G.J., E.C. Tuazon, R.A. Graham, T.M. Mischke, A.M. Winer and J.N. Pitts "Simultaneous Concentrations of Ammonia and Nitric Acid in a Polluted Atmosphere and their Equilibrium Relationship to Particulate Ammonium Nitrate," Environmental Science and Technology 13:1416-1419 (1979).

72. Platt, U., D. Perner, A.M. Winer, G.W. Harris and J.N. Pitts "Detection of NO_3 in the Polluted Troposphere by Differential Optical Absorption," Geophysical Research Letters 1:89-92 (1980).

73. Chameides, W.L. and D.D. Davis "The Free Radical Chemistry of Cloud Droplets and its Impact on the Composition of Rain," J. Geophyical Research 87:4863-4877 (1982).

74. Appel B.R., S.M. Wall, Y. Tokiwa and M. Haik "Simultaneous Nitric Acid, Particulate Nitrate and Acidity Measurements in Ambient Air," Atmospheric Environment 14:549-554 (1980).